universität wien

MASTERARBEIT / MASTER'S THESIS

Titel der Masterarbeit / Title of the Master's Thesis

„Modifications of the first-in-class Ru(III) drug candidate BOLD-100“

verfasst von / submitted by

Maximilian Anderla BSc

angestrebter akademischer Grad / in partial fulfilment of the requirements for the degree of

Master of Science (MSc)

Wien, 2020 / Vienna 2020

Studienkennzahl lt. Studienblatt / degree programme code as it appears on the student record sheet:	UA 066 862
Studienrichtung lt. Studienblatt / degree programme as it appears on the student record sheet:	Masterstudium Chemie
Betreut von / Supervisor:	o. Univ.-Prof. Dr. Dr. Bernhard K. Keppler
Mitbetreut von / Co-Supervisor:	DI Dr. Wolfgang Kandioller

Acknowledgements

I would like to thank

o. Univ.-Prof. Dr. Dr. Bernhard K. Keppler for the opportunity to write my master's thesis in his working group and for providing the intriguing topic.

DI Dr. Wolfgang Kandioller for the supervision and his continuous encouragement and guidance throughout my bachelor's and master's thesis

The NMR service team and in particular ao. Univ.-Prof. Dr. Mag. Markus Galanski for the measurement of NMR spectra during these unusual times.

Dipl.-Ing. (FH) Alexander Roller and Natalie Gajic for their expertise in X-ray diffraction data collection and structure refinement.

The staff of the Mass Spectrometry Centre and the Microanalytical Laboratory of the University of Vienna for the measurement of numerous samples.

Mag. Elfriede Limberger and Mag. Veronika Knoll for their administrative help.

Sylwia Kur BSc, Sabrina Unterburg, Daniel Strohhofer, Aleksandar Zecevic and Hans Plasser for their help in technical matters.

All the members of the working group for the warm welcome and the pleasant time.

Heiko, Sophia and Valentin for their endless support and patience. Thank you for being the best colleagues one could wish for.

All my friends from Upper Austria without whom I would be completely lost.

Anja for being the best girlfriend one could imagine.

My sister and my brother for making my life joyful.

My father, mother and entire family for their unwavering support throughout my studies and my whole life.

Abstract

Platinum-based coordination compounds are among the most important chemotherapeutics in cancer treatment. However, the routinely applied metal-based anticancer agents exhibit a number of severe side effects and have a limited scope of activity due to acquired or intrinsic drug resistance of certain tumor types.

Over the last decades, ruthenium complexes emerged as promising candidates for the development of antitumor agents, showing improved selectivity, a broader spectrum of activity and novel mechanisms of action. The ensuing studies culminated in the development of BOLD-100, a first-in-class ruthenium(III)-based metallodrug that has successfully completed a phase I clinical trial. Owing to compelling clinical results and the well-tolerated side effects, BOLD-100 was subsequently granted an orphan drug designation for pancreatic cancer. The mechanism of action of this compound is assumed to involve activation under the hypoxic conditions of tumor tissue, hence acting as prodrug. It has been demonstrated that the metal complex downregulates the chaperone GRP78, a promising target in cancer therapy, which disables a critical survival pathway in cancer cells.

Driven by the success of this novel compound class, considerable efforts in the variation of the axial *N*-donors have been made. However, there are no literature reports on leaving group or metal center modification to the best of our knowledge. Over the course of this master's thesis, seven complexes with the general formulae **A** *trans*-$[M^{III}X_4(HInd)_2]$ and **B** *trans*-$[Ru^{III}(HInd)_2(L\cap L)_2]$, where M = Ru/Rh, X = Br, Cl, HInd = 1*H*-indazole and L∩L = bidentate motif, have been synthesized. The octahedral complexes were characterized by standard analytical methods (NMR spectroscopy, ESI-MS, and elemental analysis) and the coordination motif of three complexes unambiguously confirmed by single crystal X-ray crystallography. The impact of different leaving groups and the metal centre on the electrochemical behavior was investigated by cyclic voltammetry. Studies on the stability of the complexes in aqueous solution under different conditions were performed by means of UV-vis spectroscopy. The obtained results revealed the significance of the ligand sphere and metal centre on the physicochemical properties of this promising lead structure.

Zusammenfassung

Platin-basierte Koordinationsverbindungen gehören zu den wichtigsten Chemotherapeutika in der Behandlung von Krebs. Die routinemäßig eingesetzten metallbasierten Krebsmedikamente weisen jedoch eine Reihe schwerer Nebenwirkungen auf und haben aufgrund der erworbenen oder intrinsischen Resistenzen bestimmter Tumorarten einen eingeschränkten Wirkungsbereich. Im Laufe der letzten Jahrzehnte haben sich Rutheniumkomplexe als vielversprechende Kandidaten für die Entwicklung von Antitumor-Wirkstoffen herauskristallisiert, da diese eine höhere Selektivität, ein breiteres Wirkungsspektrum und einen neuartigen Wirkmechanismus aufweisen. Die darauf folgenden Untersuchungen gipfelten in der Entwicklung von BOLD-100, einer Ruthenium(III)-basierten Metallverbindung, das bereits eine klinische Studie der Phase I erfolgreich abgeschlossen hat. Aufgrund der überzeugenden Ergebnisse und der geringen Nebenwirkungen wurde BOLD-100 anschließend der Orphan-Drug-Status für Bauchspeicheldrüsenkrebs zuerkannt. Es wird angenommen, dass der Wirkmechanismus dieser Verbindung eine Aktivierung unter den hypoxischen Bedingungen des Tumorgewebes beinhaltet und diese somit als Prodrug wirkt. Zudem konnte gezeigt werden, dass der Metallkomplex das Chaperon GRP78, welches ein vielversprechendes Ziel in der Krebstherapie ist, herabreguliert, womit ein kritischer Überlebensmechanismus in den Krebszellen inaktiviert wird.

Durch den Erfolg dieser neuartigen Verbindungsklasse wurden erhebliche Anstrengungen bei der Variation der axialen *N*-Donoren unternommen, allerdings sind in der Literatur keine Berichte über die Modifikation der Abgangsgruppen und des Metallzentrums zu finden. Im Verlauf dieser Masterarbeit wurden sieben Komplexe mit den allgemeinen Formeln **A** *trans*-$[M^{III}X_4(HInd)_2]$ und **B** *trans*-$[Ru^{III}(HInd)_2(L\cap L)_2]$ synthetisiert, wobei M = Ru/Rh, X = Br, Cl, HInd = 1*H*-Indazol und L∩L = bidentater Ligand ist. Die oktaedrischen Komplexe wurden mit analytischen Standardmethoden (NMR-Spektroskopie, ESI-MS und Elementaranalyse) charakterisiert und das Koordinationsmotiv von drei Komplexen durch Röntgenkristallographie eindeutig bestätigt. Der Einfluss verschiedener Abgangsgruppen und des Metallzentrums auf das elektrochemische Verhalten wurde mittels Cyclovoltammetrie untersucht. Untersuchungen zur Stabilität der Komplexe in wässriger Lösung unter verschiedenen Bedingungen wurden mittels UV-Vis-Spektroskopie durchgeführt und zeigten den Einfluss der Ligandensphäre und des Metallzentrums auf die physikochemischen Eigenschaften dieser vielversprechenden Leitstruktur.

Table of Contents

1 Introduction

1.1 Cancer – General Considerations

Cancer is an umbrella term describing a class of over 100 diseases characterized by abnormal cell growth, followed by invasion of surrounding tissues and potential formation of metastases.[1]

Annually over 20 000 cancer mortalities are registered in Austria, thereby representing the second leading cause of deaths in both males and females.[2] The relative impact of cancer was surpassed by premature deceases from communicable afflictions for centuries. Due to malignancies predominantly emerging at an advanced age, correlation of life expectancy and cancer incidences is well established. Comparison of life expectancy and overall deaths in Austria between 1970 and 2018 illustrate the remarkable progress of modern medicine. Notably, a substantial decrease of almost 15 000 deaths per year is reported, however, deceases attributed to malignant neoplasms increased substantially in relative as well as absolute numbers (**Figure 1**).[3,4]

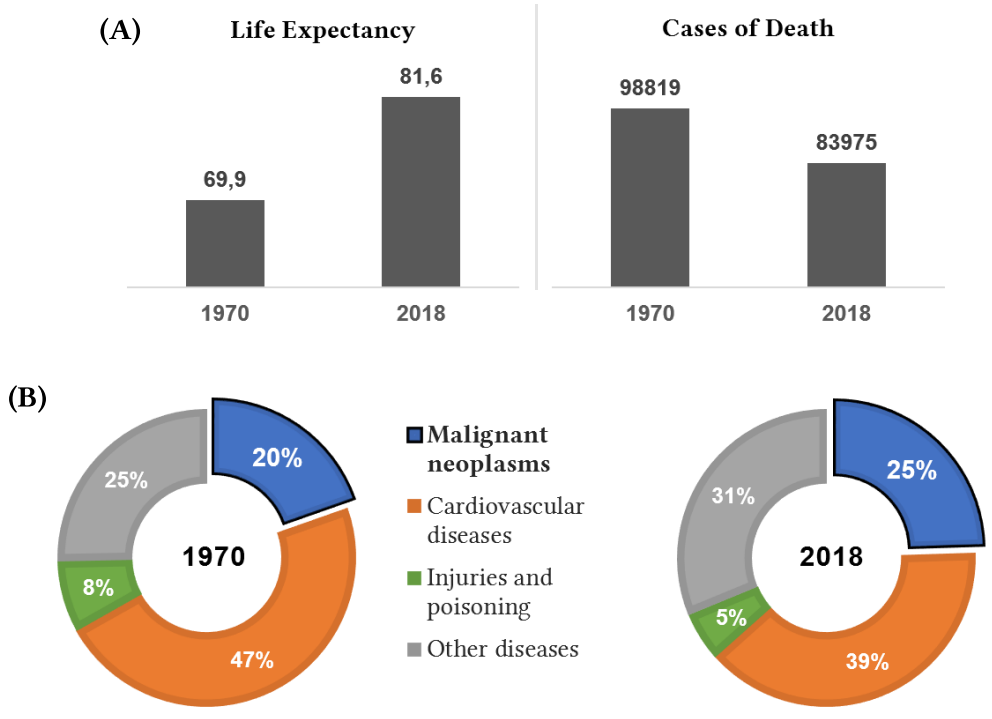

Figure 1 (A) Life expectancy and cases of death in 1970 and 2018 in Austria **(B)** Death causes in Austria in 1970 and 2018 (adapted from ref.[3,4])

The highest incidences of malignancy caused deaths (2018) among men in Austria are attributed to lung cancer (22%), followed by prostate carcinoma (11%) and colorectal carcinoma (10%). Among women, breast cancer (17%) and lung cancer (16%), followed by colorectal carcinoma (10%) are the most common.[3]

Worldwide, of the 15.2 million deaths from non-infectious diseases in 2016, 4.5 million (30%) could be attributed to malignancies. In addition, novel incidences of the global cancer burden are projected to increase by 50% in 2040, emphasizing the compelling demand for progressive cancer research to address future challenges.[5]

1.2 Causes of Cancer

All cancers emerge from multiple mutations in normal cells that translate into uncontrolled cell proliferation.[6] The determining causes triggering these mutations can be divided into endogenous and external factors. Endogenous or genetic factors include aspects of hereditary origin such as inherited mutations, hormones and reactive oxygen species (ROS) from cellular metabolism. External factors comprise carcinogens present in tobacco, diet, infectious agents and other promotors such as radiation, stress and physical inactivity. Merely 5–10% of all cancers can be assigned to genetic factors, whereas the decisive factors for malignant-cell transformations arise from external nature (90–95%, **Figure 2**).[7]

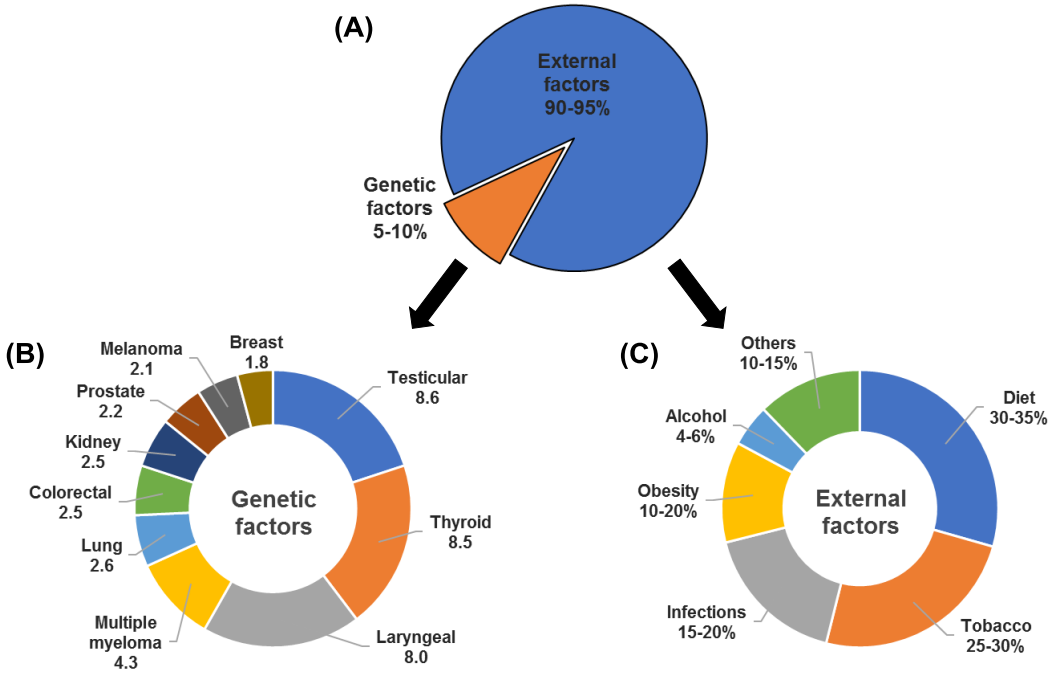

Figure 2 (A) Influence of genetic and external factors on cancer development. **(B)** Age-adjusted risk ratios of first-degree relatives of cancer cases compared with general population. **(C)** Contribution of various external factors. Adapted from ref.[7]

Based on numerous surveys, certain lifestyles considerably foster the accumulation of severe genetic alterations. The relevance of one's environment in the development of malignant diseases was also demonstrated in studies of monozygotic twins.[8] Nevertheless, these findings indicate that many cancers can be prevented within certain limits. Tobacco smoking, for instance, is the global leading avoidable cause of cancer and can be attributed to 2.4 million cancer deaths per year. On a worldwide scale, 25% of men and 5% of women are daily smokers.[9] Cigarette smoke contains more than 70 known carcinogens (*e.g.* polycyclic aromatic hydrocarbons and nitrosamines), hence increasing the risk for lung cancer 24-fold compared to non-smokers.[10] Furthermore, consumption of tobacco products is projected to cause up to 1 billion deaths in the 21st century, mainly affecting low-and middle-income countries.[5]

1.3 Carcinogenesis and Cancer Traits

The transformation of normal cells into cancer cells is termed carcinogenesis and is generally considered a multi-step process.[11] The first essential step of neoplastic development is characterized by mutations in critical genes involved in key regulatory pathways, triggered by genetic or external factors. If such **initiation** events result in grave damage so that DNA-repair mechanisms or the programmed cell death (*i.e.* apoptosis) fail, the initiated cell survives the body's defence mechanisms and the mutation becomes irreversible. These genetic alterations enable the cell to respond to growth-stimulatory actions by continuous exposure to endogenous or external parameters that lead to accumulation of proliferating preneoplastic cells. This relatively long process is called **promotion** and is reversible due to its dependence on the constant presence of a promoter. Initiated tumor cells exhibit an unstable genome, thus favouring increased rates of further mutations. Consecutive *loss-of-function* mutations in tumor suppression genes and *gain-of-function* mutations in oncogenes disrupt their sensitive balance, consequently leading to uncontrolled cell growth and transformation of benign to malignant cells. In this final step termed **progression**, tumor cells invade surrounding tissue and potentially form metastases in various body areas.

In the course of carcinogenesis, cancer cells acquire biological traits that distinguish them from normal cells. The concepts of the most fundamental characteristics are therefore presented below (**Figure 3**).

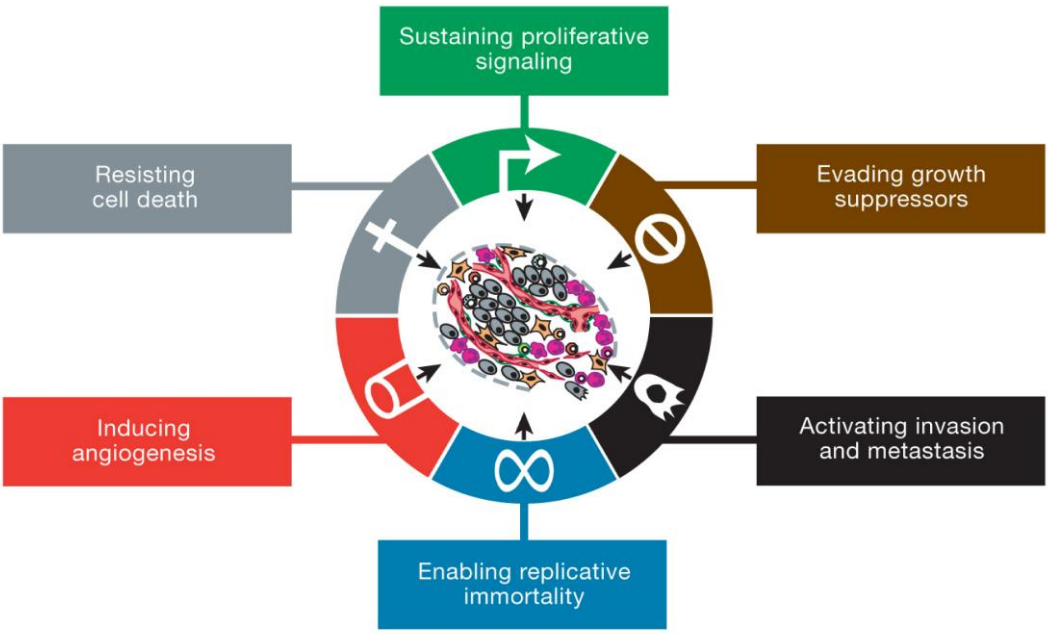

Figure 3 Major characteristics acquired by cancer cells[12]

In contrast to normal cells, cancer cells are independent from external growth signals by deregulation of different pathways, hence capable of **sustaining proliferative signalling**. Continuous proliferation is achieved for example by (i) inherent production of growth factors (*i.e.* autocrine signalling), (ii) increased expression of growth receptor proteins on the cell surface (*i.e.* hyperresponsive signalling), (iii) disruption of mechanisms responsible for preventing excessive proliferation (*i.e.* negative feedback) or (iv) somatic mutations resulting in perpetual activation of growth receptors.[13] In addition to the self-sufficiency in growth-signals, malignant cells **evade growth suppressors** that negatively regulate cell proliferation. Genetic alterations in tumor suppressor genes may lead to absence or incorrect expression of key proteins guarding the correct execution of cell division, thus enabling replication of damaged DNA. Furthermore, overgrowth of normal cells is hindered upon cell-cell contact, whereas cancer cells are insensitive to such contact inhibition.[14]

The controlled cell death by apoptosis serves as natural safeguard against tumor progression. Unnecessary or unhealthy cells are eliminated entailing activation of a family of cysteine proteases, termed caspases. Cancer cells evolved numerous tactics to avert apoptosis, hence effectively **resisting cell death**.

Downregulation of proapoptotic factors and upregulation of antiapoptotic effectors describes one of the most common strategy. The diversity of manipulating apoptotic pathways is reflected in the ability of virulent cells to modulate regulators transcriptionally, translationally, and post-translationally.[15]

Non-cancerous cells can perform only a limited number of consecutive cell divisions, followed by irreversibly entering senescence, a nonproliferative but viable state, and crisis, a state of extensive genomic instability and cell death.[16] These barriers can be attributed to a progressive shortening after each replication cycle of nucleotide sequences that protect the ends of chromosomes, termed telomeres. Tumor cells escape these limitations by expressing significant amounts of telomerase, a specific polymerase that elongates telomeric DNA, thus **enabling replicative immortality**.

All solid tissues require constant supply with nutrients and oxygen, as well as continual disposal of metabolic waste by a proper vasculature. Particularly neoplasms depend on the early **induction of angiogenesis**, a process generating new blood vessels from pre-existing ones, to grow beyond restricted size and sustain permanent proliferation. Rapid expansion of the virulent mass inevitably results in lack of oxygen (*i.e.* hypoxia) inside the tumor.[17] Hypoxia in turn triggers expression of angiogenic inducers, such as vascular endothelial growth factors (VEGF). As a result of chronically activated angiogenesis by an unbalanced mix of proangiogenic factors, neoplasms form excessive branched vascular networks with distorted and leaky vessels. Deficiencies in the vascular structure are the basis for passive accumulation of macromolecules (enhanced permeability and retention, EPR-effect).[18] In addition to secure sustenance of cancerous growths, tumor angiogenesis provides a wide interface for interactions with surrounding tissue. **Activation of invasion and metastasis** involves attenuated cell-cell adhesion capacity that enables malignant cells to escape from the primary tumor site. This angiogenic-driven process subsequently initiates the so-called invasion-metastasis cascade. Thus, cancer cells evolve abilities to penetrate tissue within the tumor's vicinity, disseminate through the circulatory system and form secondary tumor sites at distant regions of the body.[19]

Accordingly, utilization of mechanism-based therapies that target specific hallmarks of cancer permits highly increased selectivity despite less undesired side effects.

1.4 Types of Cancer Treatment

Since cancer encompasses a widespread class of diseases, diverse strategies for treatment are required. The preferred method of therapy depends on tumor type, developmental stage as well as health status of the patient. In clinical routine, therapeutic approaches are typically combined to optimize chances for cure.

The classic types of treatment include **surgery** and **radiation therapy**. Prior to such procedures, neoadjuvant therapy may be employed to reduce the size or extent of malignant growths. Adjuvant agents are administered following primary treatments for removal of tumor remnants or micrometastases. If malignant growths are too advanced or complex for treatment, palliative care aims to optimize life quality and prolong lifetime. Surgery and radiation therapy are suitable for solid primary tumors and localized metastases. However, high-energy radiation causes severe side effects, damaging both cancer and normal cells. Additionally, complete removal of the malignant growths *via* surgery or radiation is limited to non-invasive, localized neoplasms. Concerning metastases or invasive tumors, more sophisticated methods of treatment are required. Therefore, chemotherapy is a fundamental backbone to effectively neutralize cancer.

Chemotherapy in general describes the systemic treatment of malignant cells by administration of (cytostatic) drugs. The modern era of chemotherapy originated from the discovery of nitrogen mustard and its therapeutic potential in the 1940s. Since then, a plethora of anticancer agents were developed and a multi-billion dollar industry was established.[20] The cytotoxicity of chemotherapeutics is based on interference with metabolic or replicative processes of cells. A major drawback of most anticancer compounds is unselective targeting of rapid dividing cells, causing severe damage to all tissues with high replication rates (*e.g.* mucous membranes, bone marrow, hair follicles and the gastrointestinal tract).[21] Enhanced drug designs employ so-called prodrugs, a precursor of a chemical compound that is transformed *in vivo* into its active opponent.[22]

Novel concepts for cancer treatment include **immunotherapy** and **targeted therapy**. Immunotherapy specifically targets the stimulation of the endogenous immune system against malignant cells.[23] Targeted drug treatment focuses on pathways that distinguish malignant from normal cells, and interfere with molecular targets involved in specific signal transduction routes.[24]

1.5 Classes of Chemotherapeutics

Chemotherapy belongs to the class of pharmacotherapy which describes the treatment of diseases using pharmaceutical drugs. Clinical relevant chemotherapeutic agents can be classified according to their mechanism of action and are represented by several main groups of drugs:[21]

- **Alkylating agents** form highly unstable electrophilic intermediates that readily react with nucleophilic moieties. Hence, cell replication is hindered *via* covalent linkage of nucleic acids resulting in DNA strain breaks, cross-linking of DNA, RNA and proteins. Classical alkylating agents involve nitrogen mustards (*e.g.* Cyclophosphamide), nitrosoureas (*e.g.* Lomustine) and alkyl sulfonates (*e.g.* Busulfan).
- **Antimetabolites** mimic the molecular structure of enzymic substrates involved in DNA synthesis and induce cell cycle arrest. Folic acid analogues disrupt the synthetic chain of purine and pyrimidine bases (*e.g.* Methotrexate) whereas DNA base analogues terminate the assembly of the DNA double helix during replication and transcription (*e.g.* Capecitabine).
- **Topoisomerase inhibitors** block the function of essential enzymes that catalyze unwinding of DNA prior to cell replication, *e.g.* Irinotecan (toposiomerase I) and Doxorubicin (topoisomerase II).
- **Mitotic inhibitors** disrupt microtubules, impeding the separation of sister chromatids during cell proliferation. These compounds are derived from natural substances and comprise vinca alkaloids (*e.g.* Vinblastine) and taxanes (*e.g.* Paclitaxel).
- **Protein kinase inhibitors** affect central signalling pathways in cancer cells and comprise two major classes: Monoclonal antibodies that block the extracellular domain of receptor protein kinases (*e.g.* Cetuximab) and small molecule inhibitors that enter the cell and block the ATP-binding pocket of the cytoplasmic catalytic kinase (*e.g.* imatinib).

Other therapeutic strategies involve aromatase inhibitors (*e.g.* anastrozole) for the treatment of hormone-induced cancers or anticancer antibiotics.

1.6 Metals in Medicine

Metal ions hold key roles in biological systems including oxygen transport, osmotic balance, catalytic activity and structural functions in crucial enzymes. About 20 elements are essential for the human body to function properly and among them, at least 10 are metals. Accordingly, the vital metal ions for life are composed of bulk metals comprising four main group elements (*i.e.* Na, K, Ca and Mg) and transition metals (*i.e.* Mn, Fe, Co, Cu, Zn and Mo), latter commonly referred to as trace elements. The impact of inorganic trace elements on physical health is highlighted by characteristic occurring deficiency symptoms, *e.g.* Mn deficiency results in infertility and impaired skeletal growth, lack of Fe or Co leads to pernicious anaemia.[25]

The concept of utilizing metals for health and healing can be traced back thousands of years. Medicinal application of copper to reduce inflammation and iron for treating anaemia was found in the Ebers Papyrus which dates back to 1500 BC.[26] Arsenic-based compounds have been known for centuries as an effective remedy for blood diseases, bacterial and viral infections, with *Trisenox* (As_2O_3) being approved in 2000 by the FDA for the treatment of promyelocytic leukemia (APL).[27] Today, numerous metal-based agents are in clinical use to treat *e.g.* arthritis (Auranofin)[28], bipolar disorder (Li_2CO_3)[29] or applied as **anticancer agents** (*vide infra*).

Pharmaceutical research and industry have traditionally been dominated by organic chemistry. However, the incorporation of metal ions entails several features which are unavailable to organic compounds. **Radiopharmaceuticals** are powerful tools in the clinical diagnosis of malignant growths, cardiologic or neurologic disorders and organ damages. Among these, ^{99m}Tc is the most common employed radionuclide due to its desirable half-life ($t_{1/2}$ = 6h), comprehensive complex chemistry and ideal photon energy (enables simple detection and clear images).[30]

Furthermore, metal complexes are indispensable for magnetic resonance imaging (MRI). Differences in the relaxation of ^1H NMR resonances (mainly of water) in tissues can be used to generate images of lesions in various body regions. **MRI contrast agents** shorten the relaxation time of protons, thus vastly improving diagnostic accuracy. Clinically available contrast agents are mostly paramagnetic high spin complexes of Gd(III) (*e.g.* Magnevist and Gadavist) which bear a large number of unpaired electrons.[31]

1.6.1 Platinum-based Anticancer Agents

Until the 1970's, cancer chemotherapy exclusively involved organic compounds. The discovery of the anticancer potential of platinum-based drugs by Rosenberg marked the modern emergence of medicinal inorganic chemistry in cancer treatment.

In 1965, a seminal paper published by Rosenberg and co-workers indicated that certain electrolysis products of platinum electrodes inhibited cell division of *E. coli*.[32] This discovery was made serendipitously during incipient investigations on the effect of alternating current on growth rates of bacteria in chloride rich medium. Filamentous elongation of the cells implied that the cells were growing, but not proliferating. Notably, thorough research with proper control experiments revealed square-planar *cis*-diamminedichloridoplatinum(II) (cisplatin) as the primary active component.[33] Cisplatin finally passed clinical trials in 1978 and hence finds application in the treatment of bladder, ovarian, head and neck, lung, and testicular cancer.[34]

The astounding success of cisplatin paved the way for further research on Pt(II)-based anticancer complexes. Alterations of the labile chlorido leaving groups led to the development of carboplatin. This compound exhibits a reduced toxicity profile owing to the required cleavage of the cyclobutanedicarboxylato-ligand for activation, however myelotoxicity remained as dose-limiting side effect.[35] Replacement of the ammine-ligands afforded oxaliplatin bearing a 1,2-diaminocyclohexane chelating moiety. Like cisplatin, oxaliplatin undergoes non-enzymatic conversion *in vivo*, but displays a remarkably enhanced activity profile against many chemoresistant colorectal cancer cell lines.[36,37]

It has been estimated that approximately half of the administered chemotherapeutics today include platinum-based compounds as a part of combination therapy.[38] Despite considerable progress made in the development of novel platinum complexes (including octahedral Pt(IV) compounds), cisplatin, carboplatin and oxaliplatin currently remain the only platinum-based anticancer agents with worldwide approval (**Figure 4**).

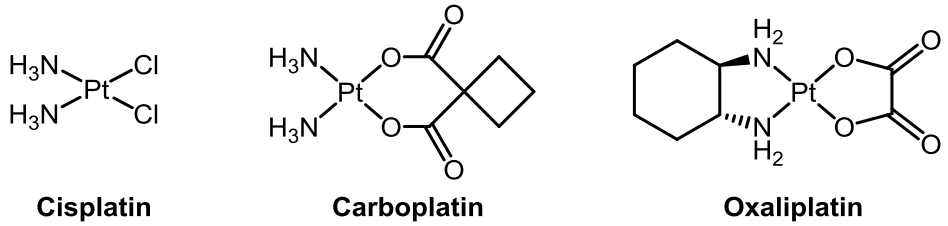

Figure 4 Worldwide approved platinum-based compounds

Cisplatin is commonly administered intravenously as acidic saline solution (Platinol®) and interactions of the compound with biological components are of great importance (**Figure 5**). A major fraction (up to 98%) binds irreversibly to abundant serum proteins, thus inactivating the drug.[36] Particularly human serum albumin (HSA) is known to form platinum-adducts by virtue of nucleophilic cysteine, methionine and histidine residues.[39] Cisplatin enters fast dividing cells mainly *via* passive diffusion, followed by replacement of the chlorido ligands with labile aqua ligands. Intracellular aquation is facilitated by significant differences in extracellular (~105 mM) and cytoplasmic (~4 mM) chloride concentration.[40]

This activated species is a potent electrophile that readily reacts with electron-rich sites of biomolecules such as DNA, RNA and proteins. In fact, cytotoxic effects are primarily mediated *via* DNA adduct formations which arise from interactions with nucleophilic *N*7 of guanine and adenine. More than 80% of total platinum-DNA damage can be attributed to 1,2-intrastrand GpG and ApG adducts. Other lesions comprise 1,3-intrastrand GpG adducts, GpG interstrand crosslinks and monoadduct formations.[41] These pseudo-alkylations lead to structural distortions of the DNA that inhibit the recognition of enzymes which are crucial for cell replication, ultimately resulting in cell death.

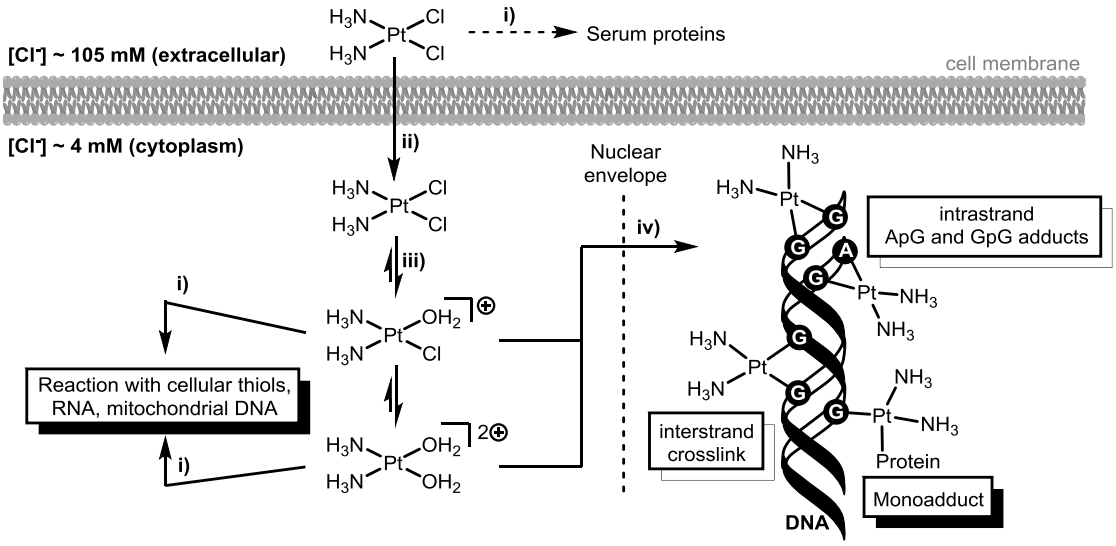

Figure 5 Schematic overview of cisplatin interactions *in vivo*: **i)** Undesired cytoplasmic or extracellular drug inactivation, **ii)** cell uptake mediated *via* passive diffusion, **iii)** aquation triggered by low intracellular chloride concentration generates activated species, **iv)** DNA-adduct formation

However, cisplatin therapy entails numerous undesirable side effects including neurotoxicity, myelosuppression and dose-limiting nephrotoxicity.[42] In addition, acquired or intrinsic resistance of many tumors against Pt(II)-based anticancer agents limits the range of treatable cancer types.[43] These drawbacks prompted further research on antineoplastic non-platinum metal complexes, aiming for increased selectivity, a broadened profile of activity and an altered mechanism of action.

1.7 Ruthenium Complexes as Antitumor Agents

Ruthenium is a d-block metal and, along with osmium and iron, a member of group 8 in the periodic table. The main field of application in chemistry was primarily catalysis until its anticancer properties were found out more than eight decades ago.[44] Ruthenium complexes are currently one of the most promising alternatives to platin and are expected by several researchers to become the next generation of clinical metal-based anticancer agents.[45] The physiologically relevant profile of ruthenium lends itself to medicinal application, which is therefore presented below:[46,47]

First, ruthenium-derived complexes possess an easily fine-tuneable rate of ligand substitution, dictated by the coordination sphere of the complex. **Ligand-exchange kinetics** in ruthenium complexes are in the order of minutes to hours which is comparable to the timescale of cellular processes. Furthermore, ruthenium exhibits **multiple accessible oxidation states** (II and III) under physiological conditions. In these oxidation states, ruthenium complexes tend to adopt octahedral geometry which offers a higher versatility of possible ligand systems in contrast to square-planar coordination spheres of Pt(II). In addition, it has been shown that ruthenium-complexes can bind to serum transferrin (*i.e.* an iron-binding plasma protein).[48,49] Cancer cells have higher nutritional demands compared to normal cells, consequently leading to a higher expression of transferrin receptors on the cell surface. Transferrin-mediated uptake of ruthenium-based drugs is suspected to correlate with a **lower systemic toxicity**.[50]

Most Ru(III) as well as Ru(II) complexes are low-spin, with Ru(III) having the higher value of crystal field stabilization energy (CFSE) Δ, owing to its greater charge. A higher value of Δ leads to an increased free activation energy, $\Delta G^{\ddagger}$, thus resulting in a smaller water exchange rate constant *k*. Indeed, the first order constant *k* was found to be ~10^{-2} s^{-1} ($t_{1/2}$ ~ 1 min) for aquated Ru(II) and ~10^{-6} s^{-1} ($t_{1/2}$ ~ 19h) for Ru(III) at 25°C, most likely *via* an associative mechanism.[39]

The stabilities of different oxidation states allow *in vivo* interconversion of kinetically more inert Ru(III) to its active Ru(II) counterpart, particularly favoured in the reducing environment of hypoxic tumor tissue. According to the hard and soft acid and base (HSAB) principle, Ru(II), a soft acid, and Ru(III), an intermediate acid, are considerably softer than the corresponding states of iron. Consequently, softer ligands are favoured, and particularly nitrogen donors. Hence, the imidazole residue of histidine, *N*7 of nucleobases, or the thiols of cysteines represent attractive biological targets.

The limited activity spectrum of antineoplastic platinum compounds and, in addition, resistances stimulated research on alternative transition metals. Initial observations on ruthenium complexes as anticancer agents were reported in 1976. Herein, *fac*-$[Ru^{III}Cl_3(NH_3)_3]$ induced filamentous growth of *E. coli*, but was not further investigated owing to solubility problems.[51] The ensuing studies culminated in the discovery and development of two Ru(III) lead structures that advanced to clinical trials, comprising imidazolium *trans*-[tetrachlorido(1*H*-imidazole)(*S*-dimethyl-sulfoxide)ruthenate(III) (NAMI-A, **Figure 6**) and indazolium *trans*-[tetrachloridobis(1*H*-indazole)ruthenate(III)] (KP1019, FFC14A).[52] The latter will be discussed in detail in the next section.

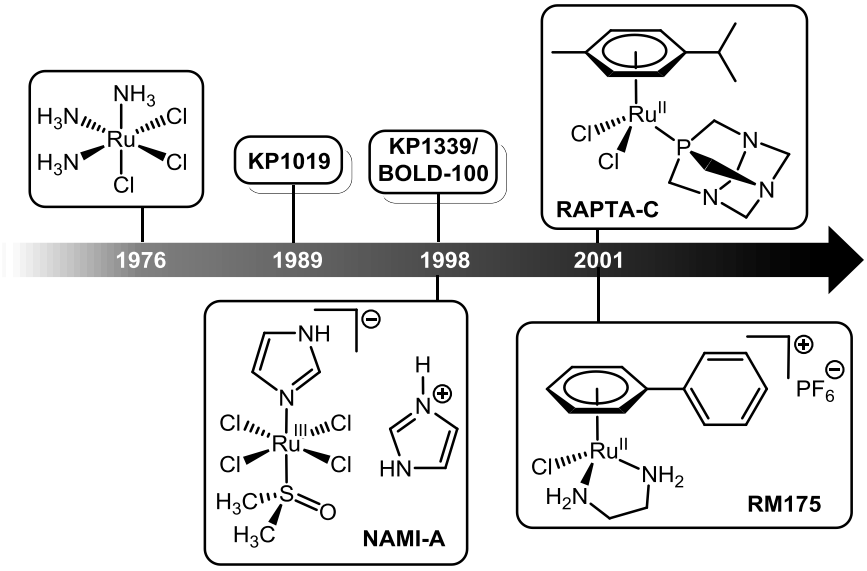

Figure 6 Timeline of the discovery of lead structures. Adapted from ref.[52]

NAMI-A exhibited limited *in vitro* cytotoxicity but showed remarkable efficacy against lung metastases in mouse models. Therefore, it was proposed that proangiogenic factors rather than DNA were the main targets. Nevertheless, clinical studies had to be terminated due to poor patient response and the development of painful blisters on the skin at higher doses.[53]

Under physiological conditions, Ru(III) complexes were found to be relatively inert towards ligand substitution, hence activation *in vivo* is required. Thus, Ru(II) was assumed as the active metal species for the mechanism of action which stimulated investigations on Ru(II)-based agents. A prime example of Ru(II) compounds are pseudo-octahedral half-sandwich complexes with so-called "piano-stool" configuration, featuring a facially η^6-coordinating arene ligand that prevents reoxidation. The first promising Ru(II)-arene based compounds were developed by Dyson *et al.* and the Sadler group including RAPTA-C and RM175 (**Figure 6**).[54,55]

It has been found that these organometallic complexes are relatively inert towards interaction with biological targets and act as prodrugs.[55,56] Similar to cisplatin, intracellular activation by replacement of the chlorido leaving group with a labile aqua ligand is supposed to be essential for the mechanism of action ("activation by aquation" hypothesis).[56] In contrast to Pt-based compounds, proteins rather than DNA are suspected to be involved as primary targets.[57]

Another approach for Ru(II)-based compounds as anticancer agents is their application as photosensitizers in photodynamic therapy (PTD). This type of treatment relies on the application of compounds that produce reactive oxygen species (ROS) and/or singlet oxygen radicals ($^1O_2$) upon activation with light.[58] The induced oxidative stress damages essential biomolecules, leading to cell death. TLD-1433, a promising photosensitizing agent, has recently entered phase II clinical trials against bladder cancer, thus demonstrating the potential of ruthenium-based compounds for clinical purposes (**Figure 7**).[59]

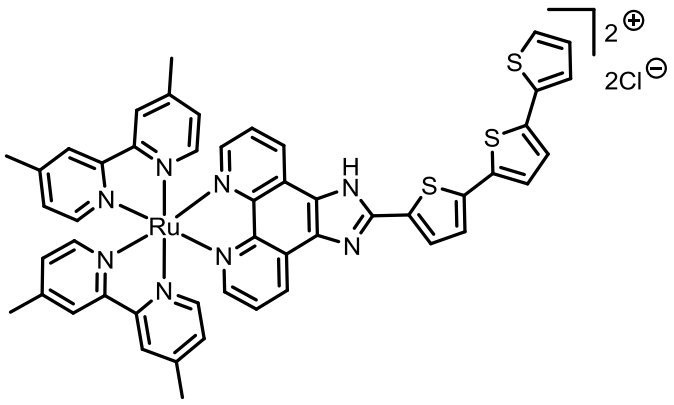

Figure 7 Structure of TLD-1433[59]

1.8 Towards KP1019 and BOLD-100

In the late 1980s, Keppler and co-workers synthesized and tested a series of ruthenium complexes in P388 leukemia mouse model.[60–62] Accordingly, the most promising and water-soluble complexes featured (HN-Het) *trans*-[$RuCl_4$(N-Het)$_2$] and (HN-Het) *trans*-[$RuCl_5$(N-Het)] scaffolds, where N-Het represents an nitrogen containing heterocycle. Further *in vivo* experiments in an autochthonous colorectal carcinoma in rats revealed that the best results were obtained with the derivative H_2Ind *trans*-[$RuCl_2$(Hind)$_2$] (**KP1019**, **Figure 8**), where Hind is 1*H*-Indazole.[63] Notably, reduction of tumor mass up to 95% without any considerable weight loss or mortalities was observed, while cisplatin remained completely inactive.

Based on these excellent antineoplastic effects, KP1019 was selected to proceed in (pre)clinical studies. In fact, the anticancer activity of KP1019 against solid tumors was confirmed in a clinical phase I dose escalation study, which showed disease-stabilization for 8–10 weeks in five of six evaluable patients beside the absence of any severe side effects.[64] However, the maximum tolerated dose (MTD) was not determinable due to limitations in solubility of the compound which prevented continuation of clinical studies.[50]

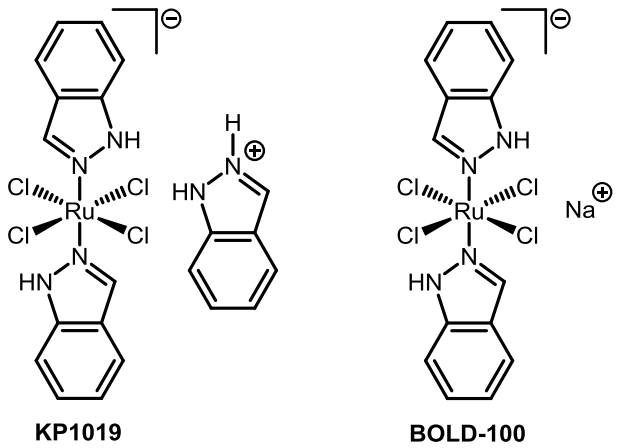

Figure 8 Structures of clinical-developed ruthenium complexes

To circumvent this problem, the indazolium counterion was replaced with sodium, yielding sodium *trans*-[$RuCl_4$(HInd)$_2$] (**BOLD-100**, formerly known as KP1339, NKP-1339 and IT-139, **Figure 8**) and increasing the solubility by a factor of 35.[65] A subsequent initiated phase I dose escalation study which included 46 patients with solid tumors refractory to standard treatment was completed successfully with encouraging results.[66]

It has been demonstrated that BOLD-100 was well-tolerated with a manageable safety profile at the MTD (determined at 625 mg/m^2), while one patient experienced partial response and nine additional patients achieved disease stabilization. These promising results combined with the limited side effects culminated in the orphan drug designation granted by the FDA in 2017 for pancreatic cancer.[67] Compelling preclinical efficacy in combination with established anticancer therapies translated into an ongoing phase 1b clinical trial of BOLD-100 with FOLFOX which opened earlier this year. FOLFOX is a standard chemotherapy regimen for the treatment of colorectal cancer and is composed of the drugs folinic acid, fluorouracil and oxaliplatin. Today, the first-in-class Ru(III) drug candidate BOLD-100 is the most advanced and promising ruthenium-based anticancer agents.

1.8.1 Plasma protein mediated drug delivery

KP1019 and BOLD-100 are administered intravenously. Rapid binding to plasma proteins was demonstrated in several studies, with less than 1% free metal complex in human blood samples taken after 20 minutes of drug administration.[50] Thus, their anticancer activity is inextricably tied to interactions with serum proteins. In particular human serum albumin (HSA) and transferrin (Tf) have been shown to exhibit strong affinities towards the latter metal-based complexes.[64] Therefore, it was proposed that drug delivery to cancer cells is mainly mediated by these two proteins. In fact, biomacromolecules such as albumin and transferrin attracted considerable attention as carriers for drug delivery in recent years.[68] Accordingly, two modes of transportation were suggested to comprehend the clinical observed tumor selectivity and low toxicity of KP1019 and BOLD-100:[69] (1) Transferrin- and (2) HSA-mediated pathways. (1) After cell uptake *via* transferrin receptor mediated endocytosis, the complex may be released from endosomes inside the cell at low pH (5-6), where the antiproliferative activity is exerted. Exceedingly high levels of transferrin receptors are frequently expressed on malignant cells due to their voracious demand on nutrients. (2) Based on the EPR-effect (see section 1.3), macromolecules of a certain size (> 40 kDa) tend to accumulate in tumor tissue. Distorted and leaky vessels facilitate transit into cancerous growths, followed by drug release after albumin degradation.[70]

Competition studies revealed that KP1019 exhibits much stronger affinities towards albumin than transferrin, but it binds faster to Tf. Therefore, adduct formation with Tf is kinetically favored, whereas HSA adducts are thermodynamically more stable.[49] Additionally, in human plasma HSA is present in a more than 10-fold excess compared to Tf. Detailed analysis of blood samples taken from a patient during clinical studies evidenced that KP1019 was almost exclusively bound to albumin.[71] Intriguingly, recent X-ray studies revealed the binding sites of KP1019 on HSA, showing two "naked" Ru atoms bound to histidine residues and coordinated octahedrally by solvent molecules.[72] In contrast to a previously reported structure of KP1019 bound to human lactoferrin, both axially coordinated indazole ligands are dissociated.[73] However, a two-step binding mechanism was proposed, demonstrating the important role of the indazole ligands despite their absence in the structure. First, the intact ruthenium complex approaches the protein *via* hydrophobic interactions of the indazole moieties. After the binding site is reached, the hydrophobic interactions are slowly converted to coordinative interactions, thus exchanging the *N*-donor ligands. A similar pathway *via* electron paramagnetic resonance experiments was suggested before,[74] and highlights the significance of the indazole heterocycles for plasma protein mediated drug delivery.

1.8.2 Mechanisms linked to anticancer activity

As mentioned in section 1.7, ruthenium occurs in two oxidation states under physiological conditions, Ru(III) and Ru(II). Owing to the small changes in bond distances of ligands between Ru(III) and Ru(II) ions, the energetic difference of the Franck-Condon barrier to electron transfer is small.[75] Therefore, interconversion of Ru(III) to Ru(II) readily occurs in the presence of reducing agents in biological media. Furthermore, reduction of Ru(III) to its Ru(II) counterpart fills the d_π (t_{2g}) orbitals. Hence, π-donor ligands (*e.g.* chlorido, hydroxido) that firmly coordinate to Ru(III) bind markedly less strongly to Ru(II), resulting in rapid ligand exchange reactions.[39] Upon reduction, exchange of the chlorido leaving groups of KP1019 and BOLD-100 by aqua ligands is considerably accelerated, resulting in an activated species with enhanced reactivity towards biomolecules.[69] Indeed, the aquation product *mer,trans*-$[RuCl_3(HInd)_2(H_2O)]$ featuring a labile Ru–OH_2 bond was isolated recently and several reactions with different donor molecules by release of H_2O were demonstrated.[76]

In addition, rapidly proliferating cancer cells are depleted of nutrients and oxygen (see section 1.3), and therefore have to rely more strongly on glycolysis. Consequently, cancerous cells excessively generate lactic acid decreasing the pH value, leading to a reductive environment within the tumor tissue.[77] These fundamentals prompted the formulation of the "activation-by-reduction" hypothesis, assuming that Ru(III) is predominantly reduced in tumor tissue and therefore acts as prodrug. Hence, *in vivo* transformation into an activated species is believed to be crucial for the anticancer activity of KP1019 and BOLD-100. In addition, formation of reactive oxygen species (ROS) *via* the redox active metal-centre was identified, causing severe damage to cancer cells by disrupting the cellular redox balance.

However, the activation-by-reduction hypothesis should be handled with caution. Several hydrolysis studies with KP1019 and BOLD-100 demonstrated that Ru(III) compounds are not particularly inert towards ligand substitution.[78,79] Furthermore, recent X-ray absorption near edge spectroscopy (XANES) experiments revealed that BOLD-100 remained entirely in its oxidized state +III in tumor tissue in mice,[80] whereas earlier studies conducted by the same group indicated that both accessible oxidation states can occur in various tissue samples.[81] Nevertheless, extensive ligand exchange reactions of Ru(III) upon interaction with biomolecules were observed in both publications.

In contrast to platinum-based anticancer agents, DNA damage is not assumed to be the primary cause of the anticancer properties of KP1019 and BOLD-100. Recent studies demonstrated that BOLD-100 triggers disruption of endoplasmic reticulum (ER) homeostasis *via* depletion of key cellular chaperones including the 78-kDa glucose-regulated protein (GRP78).[82] Under ER stress, misfolded proteins accumulate, and GRP78 alleviates their aggregation, ultimately initiating the unfolded protein response (UPR). Notably, the UPR represents an evolutionarily conserved adaptive response which is an important survival pathway for cancer cells to overcome proteotoxic stress.[83] In carcinogenesis, upregulation of GRP78 is a result of intrinsic and extrinsic factors, such as hypoxia and a decreased pH value in the tumor microenvironment. Elevated levels of GRP78 are associated with angiogenesis, tumor metastasis, drug resistances, and cell survival. Therefore, GRP78, the master regulator of UPR, is as an emerging target for cancer therapy. Bakewell and co-workers showed that BOLD-100 exhibits striking activity in the suppression of GPR78 expression in cancer cells, while normal skin cells adjacent to the tumor were not affected.[83]

A simplified overview of the intricate *in vivo* behaviour of BOLD-100 is illustrated below (**Figure 9**).

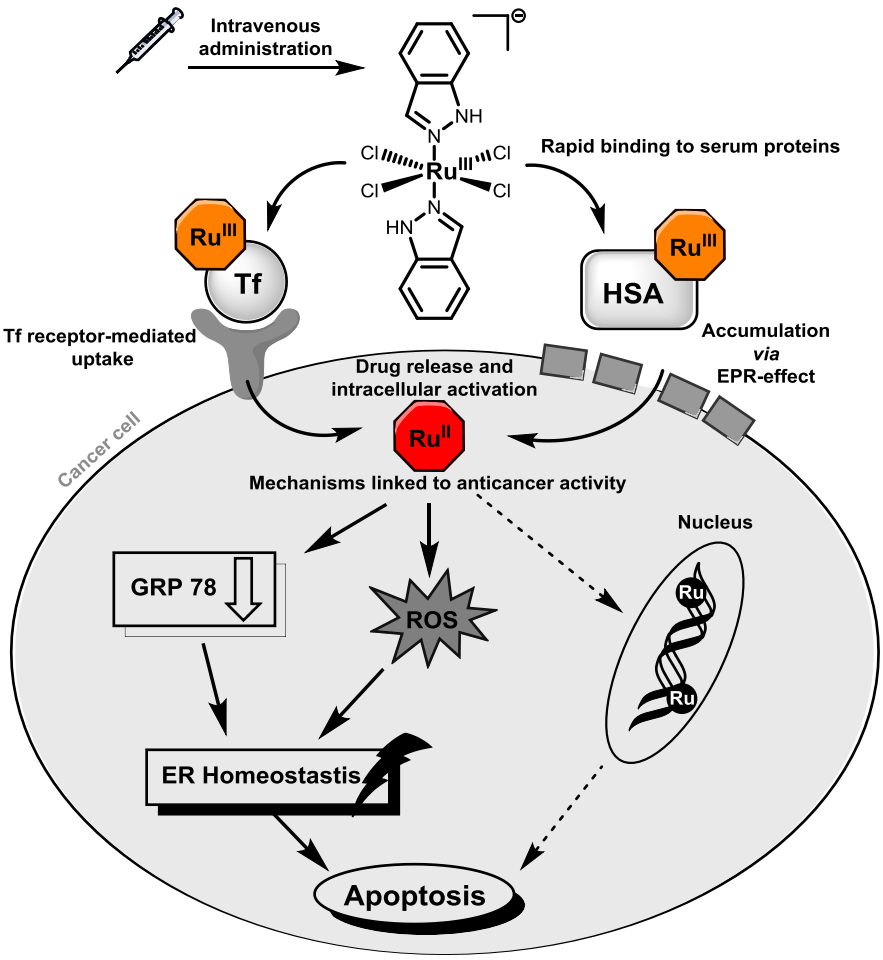

Figure 9 Schematic overview of *in vivo* interactions and mechanisms linked to the anticancer activity of BOLD-100

In conclusion, the exact mode of action of KP1019 and BOLD-100 is complex and still not completely understood. Intensive research on molecular targets is ongoing to support the further clinical development of this first-in-class ruthenium-based agent.

1.8.3 Reported Lead Structure Modifications

Driven by the success of the novel compound class *trans*-[$RuCl_4$(N-Het)$_2$], considerable efforts have been made in the variation of the axial *N*-donor ligands. These complexes include, but are not limited to:

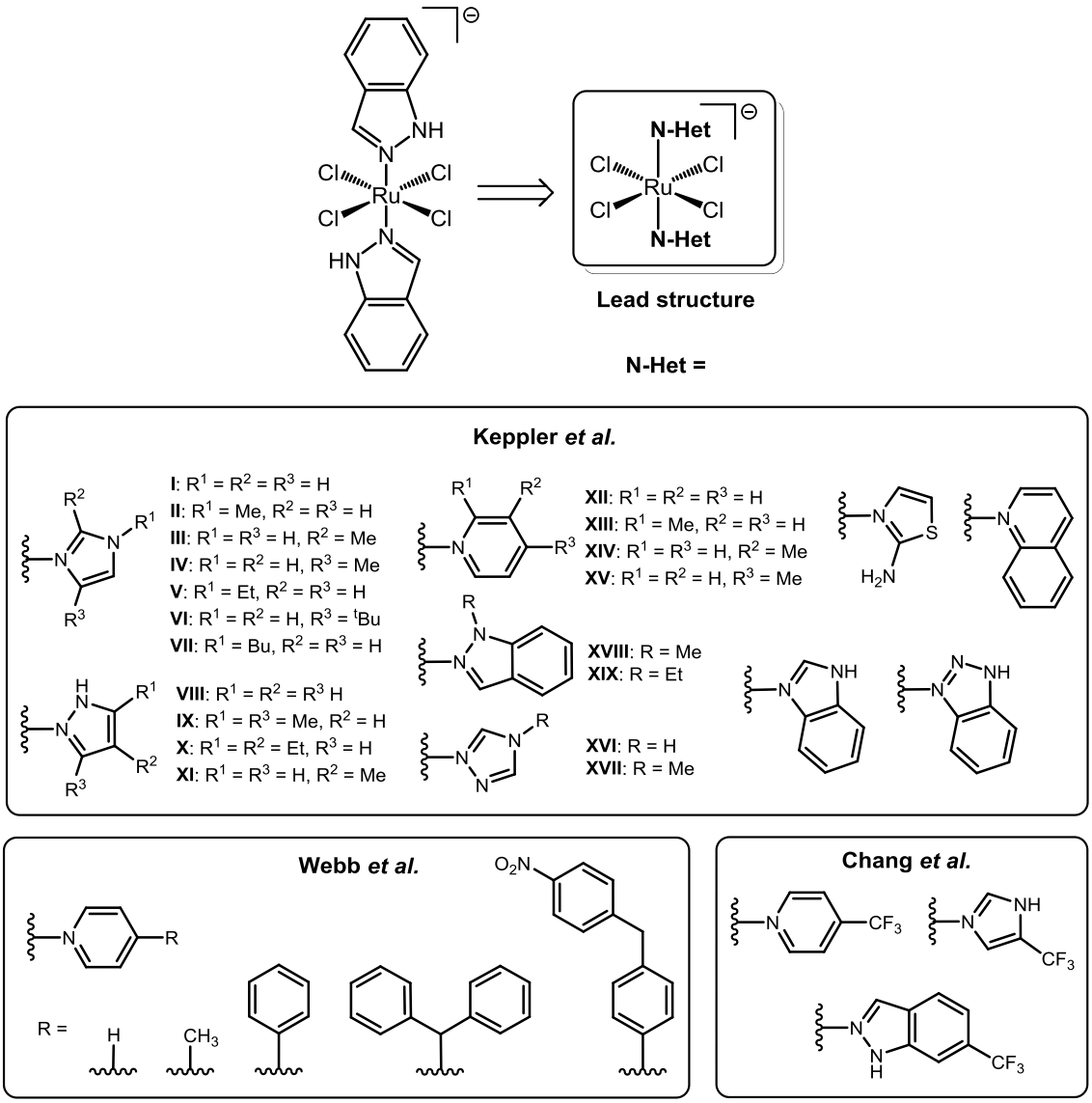

Figure 10 Reported *N*-donor variations of the lead structure[63,84–87]

No substantial improvements concerning *in vitro* or *in vivo* anticancer activity were achieved, thus rendering 1*H*-indazole as the best suited heterocyclic ligand of this promising lead scaffold.

2 Results and Discussion

The goal of this thesis was to synthesize derivatives of BOLD-100 by substitution of the chlorido ligands and variation of the metal center. Also, there are no literature reports on leaving group or metal center modification to the best of our knowledge. Despite compelling results obtained from clinical trials, the exact mechanism of action is still unknown and limited stability under physiological conditions complicate approval for clinical application. Accordingly, the results presented within this work give insight into the impact of the leaving groups and metal center on the physicochemical, and ultimately anticancer properties.

Previously reported alterations of the *N*-donors confirmed the lead structure featuring *trans*-coordinated 1*H*-indazole heterocycles to the Ru(III) core. Thus, two different approaches comprising scaffolds of the general formulae **A** *trans*-[$M^{III}X_4(HInd)_2$] and **B** *trans*-[$Ru^{III}(HInd)_2(L{\cap}L)_2$] were considered (**Scheme 1**). Halide exchange and metal center variation are promising approaches to fine-tune ligand substitution kinetics and alter the redox behavior of a complex.[56,88] Replacement of the chlorido leaving groups by a bidentate motif may increase *in vivo* stability due to the chelate effect.

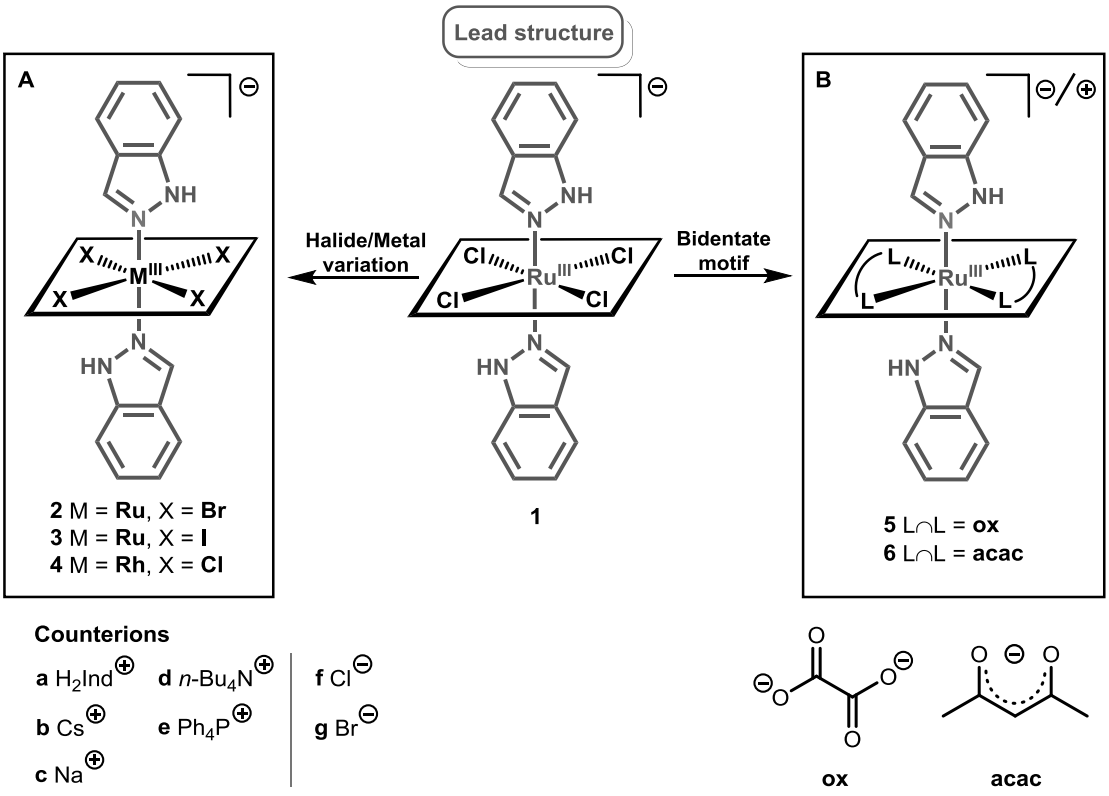

Scheme 1 Aspired complexes in the course of this thesis

2.1 Synthesis

2.1.1 Synthesis of KP1019 (**1a**) and BOLD-100 (**1c**)

First, KP1019 and BOLD-100 were synthesized as reference compounds and used as starting material for further reactions. Preparation was conducted according to the reported patent procedure (**Scheme 2**).[89] $RuCl_3.xH_2O$ is refluxed in ethanol and concentrated hydrochloric acid for purification. The obtained solution containing exclusively Ru(III) is then reacted with 1*H*-indazole in concentrated HCl yielding **1a**. Further reaction of crude **1a** in a mixture of methyl ethyl ketone (MEK) and EtOH with an excess of CsCl afforded the corresponding Cs-salt **1b**. The obtained material contained **1b** as MEK solvate and was converted to its more stable hydrate by combining the complex salt with a mixture of ethanol and H_2O. Compound **1b** was obtained as red-brown microcrystalline solid in excellent yield (85%). Subsequent stirring of a suspension containing the Cs-salt **1b** and 1.1M $NaAl(SO_4)_2$ provided the desired Na-salt **1c** as voluminous brown powder in good yield (83%).

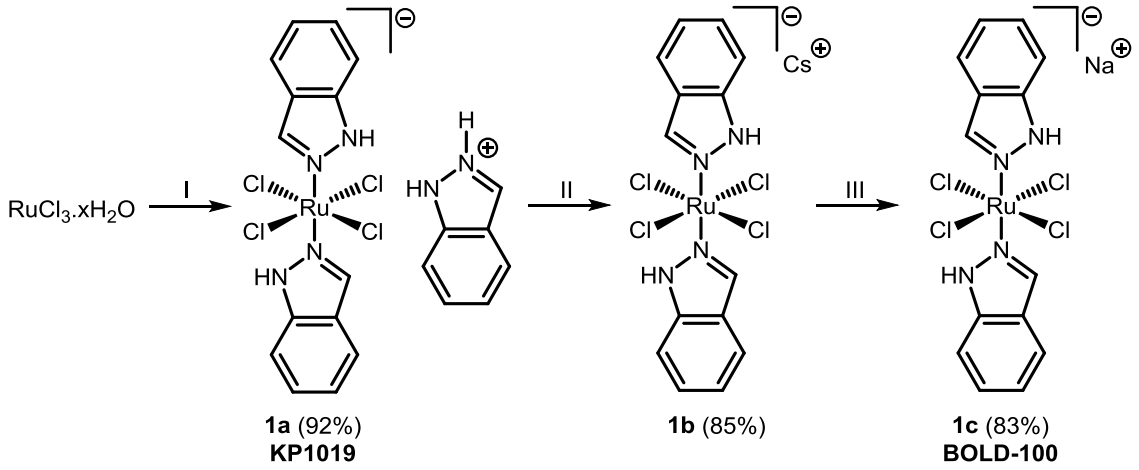

Scheme 2 Synthesis of BOLD-100[89]
(I) i) = HCl conc., EtOH, T = reflux, t = 2 h; ii) = 1*H*-Ind (6.64 eq), HCl conc., T = 85 °C, t = 10 h;
(II) i) = CsCl,(2.8 eq), MEK/EtOH (10:9), T = r.t., t = 2 h; ii) = EtOH/H_2O (2:1), T = r.t., t = 15 min;
(III) 1.1 M $NaAl(SO_4)_2$, T = r.t., t = 48 h

In order to isolate **1a**, a procedure adapted from Lipponer *et al.* was employed.[90] Thus, **1a** was stirred in H_2O to remove excess HCl and was isolated by filtration in excellent yield (92%). However, KP1019 is difficult to isolate as a pure substance free of solvent, and filtered material contained residual water and hydrochloric acid. Furthermore, drying or washing the crude product with polar solvents (*e.g.* ethanol) induced degradation. Therefore, crude **1a** was converted directly to **1b** without purification, increasing product purity and overall yield (65%) substantially.

Application of a MEK/EtOH mixture resulted in the formation of a crystalline MEK solvate of the caesium salt **1b**, which facilitated isolation eminently without any observable degradation in contrast to **1a**. Preparation of **1b** as an intermediate is a crucial step towards the synthesis of **1c**, thus favoring this synthetic route over existing methods. Conversion of the caesium salt **1b** to the desired complex **1c** proceeded by precipitation of the formed water insoluble caesium aluminium sulfate which was continuously removed from the reaction mixture, hence shifting the equilibrium towards formation of the sodium salt **1c**.

2.1.2 Synthesis of complex salts **2**

Several synthetic approaches were investigated in order to synthesize the bromido-analogue **2**. The first conducted procedures comprised halide exchange reactions employing **1a**, **1b** or **1c** with bromide alkali metal salts (NaBr, KBr or CsBr) and heating at reflux in ethanol (99%). Unfortunately, the performed reactions yielded dark green solutions with a variety of not assignable products, hence the desired complex was not obtained. Therefore, different strategies involving $RuBr_3$ as starting material were employed.

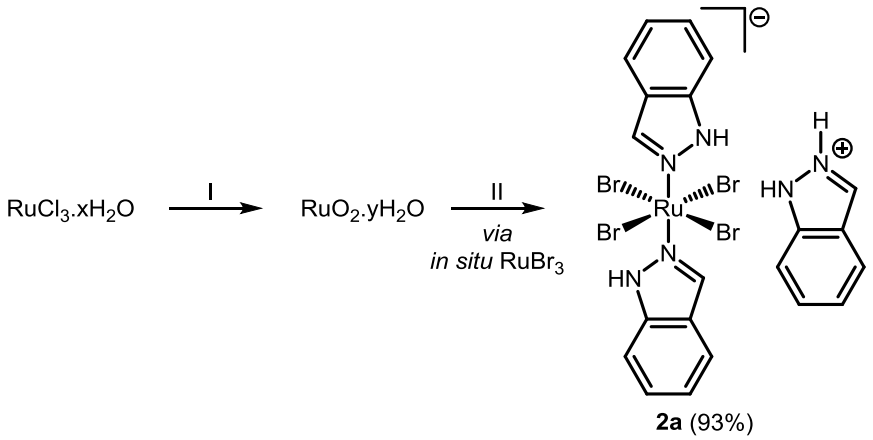

Scheme 3 Synthesis of **2a**
(I) H_2O, 10 M NaOH, T = reflux, t = 30 min;
(II) i) = HBr conc., T = 0° C, t = 1 h; ii) = EtOH, T = reflux, t = 2 h; iii) = HBr conc., 1*H*-indazole, T = 85 °C, t = 16 h

Crutchley *et al.* reported a simple procedure for the preparation of *in situ* generated RuX_3 (X = Br, I).[91] Herein, commercially available $RuCl_3.xH_2O$ was dissolved in H_2O and reacted with 10 M NaOH under reflux to $RuO_2.yH_2O$. The black oxide was filtered, washed with acetone and water, and subsequently suspended in a beaker with concentrated HX (X = Br, I) at 0°C until all solids were dissolved.

This procedure afforded *in situ* generated RuX_3 which was utilized as source material for further reaction. In order to synthesize **2a**, the crude $RuBr_3$-solution required purification to remove small amounts of Ru(IV) and other impurities.[63] Thus, the mixture was combined with non-denatured ethanol and heated at reflux, followed by distillation to remove formed acetaldehyde and excess ethanol. This purification step proved to be essential since reactions with the crude solution did not yield any product.

The concentrated Ru(III)-mixture was then added dropwise to a solution containing 1*H*-indazole (8 eq.) dissolved in concentrated HBr and stirred overnight at 85 °C (**Scheme 3**). It was observed that a large excess of 1*H*-indazole and at least 16 hours of reaction time are required to achieve reproducibly high yields. The collected precipitate was washed with 2 M HBr to separate remaining 1*H*-indazole and stirred in H_2O to remove excess HBr. Filtration and drying *in vacuo* afforded **2a** as a purple microcrystalline solid in excellent yield (93%).

As observed for **1a**, **2a** could not be isolated free from impurities as it contained residual water and hydrobromic acid. Washing with ethanol or diethyl ether was impractical, leading either to considerable loss of yield or product degradation. In addition, heating of **1a** in THF or ethyl acetate led to the formation of the neutral, meridionally coordinated complex **2*** [$RuBr_3HInd_3$], presumably *via* Anderson-type rearrangement (**Scheme 4**).[92] It can be hypothesized that the proton migrates from the indazolium cation to a coordinated bromido ligand, thus leaving as HBr from the complex. The resulting vacancy is then substituted by the deprotonated 1*H*-indazole moiety.[93]

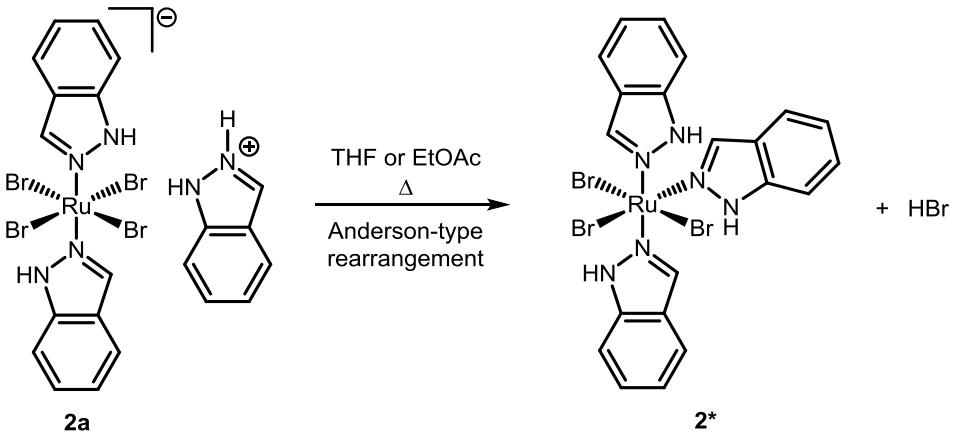

Scheme 4 Rearrangement of **2a** observed in THF or EtOAc

The novel synthesized complex **2a** was hardly soluble in water. In addition, **2a** proved to be unstable in various organic solvents, undergoing undesired rearrangement reactions (*vide supra*). Thus, synthesis of the sodium analogue **2c** was probed to improve the water solubility which is essential for further *in vitro* and *in vivo* experiments. It has been reported that the primary degradation product of the chlorido-analogue **1a** is caused by an aquation reaction that is considerably accelerated in alkaline aqueous solutions (see section 1.8.2).[89] To avoid premature transformations, **2a** was employed as crude and wet product for further reactions in order to improve the stability of the complex by the presence of residual hydrobromic acid.

Initial experiments to synthesize **2b** based on the original patent procedure[89] were unsuccessful as a clear solution remained without precipitation of the MEK solvate. In a procedure reported by Peti *et al.*, **1c** is prepared by salt metathesis of the tetra(*n*-butyl)ammonium **1d** or tetraphenylphosphonium **1e** complex salts *via* treatment with sodium tetraphenylborate.[65] In order to synthesize **2d** and **2e**, a similar method with slight adaptions was utilized (**Scheme 5**). Herein, **2a** was dissolved in a mixture of H_2O and acetone or methanol, followed by the addition of the respective bromide salts. Immediate precipitation of the complexes as pink solids was observed. After filtration and washing with water, the pink solids were obtained in good to excellent yields (**2d** 88%, **2e** 67%). The use of methanol in the case of **2e** increased the moderate yield of 52% substantially.

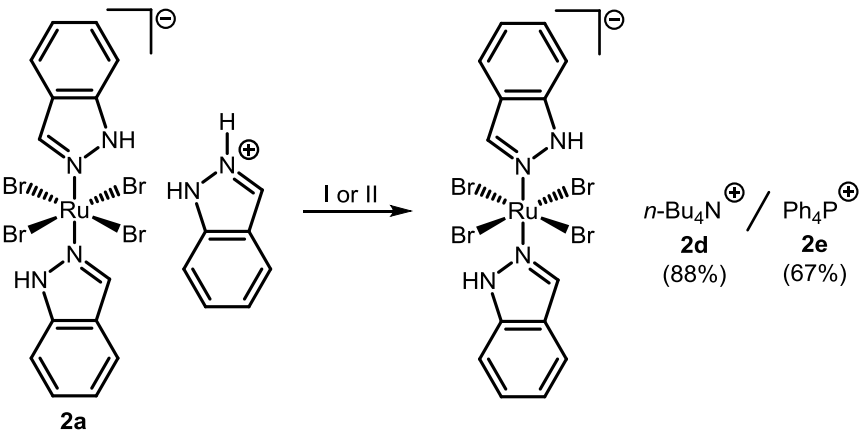

Scheme 5 Preparation of complex salts **2d** and **2e**
(I) Synthesis of **2d**: *n*-Bu_4NBr (4 eq.), acetone, H_2O, T = r.t., t = 4 h;
(II) Synthesis of **2e**: Ph_4PBr (4 eq.), MeOH, H_2O, T = r.t., t = 4 h

Differences in solubility characteristics mediated by the lipophilic counterions of **2e** and **2d** were utilized for the synthesis of the comparatively polar compound **2c**. Subsequently, sodium tetraphenylborate was added to the complex salts **2d** and **2e** in acetonitrile, leading to precipitation of the corresponding tetraphenylborate salts.

In contrast to the published procedure, the desired complex **2c** did not precipitate upon addition of diethyl ether, presumably due to increased lipophilicity mediated by the bromido-ligands. Consequently, the crude material was dissolved in THF and precipitated with *n*-hexane. Unfortunately, the obtained product contained residual tetraphenylborate impurities, as confirmed by ^{1}H NMR and ESI-MS. Synthesis of complex **2** compensated by the tetramethylammonium cation for the application on cation exchange resins as described in the literature was also unsuccessful.[65] Therefore, other strategies were considered to afford **2c** in sufficient purity.

Thorough investigation revealed that an increased ratio of ethanol is essential for the formation of the crystalline MEK solvate of **2b**. Thus, synthesis of the MEK solvate of complex **2b** was achieved by combining **2a** with CsBr (3.3 eq.) and a mixture of EtOH/MEK 3:1, followed by treatment with aqueous ethanol to afford the corresponding hydrate. Monitoring of the reaction process *via* ^{1}H NMR spectroscopy showed only partial conversion even after a prolonged reaction time (48 h). The residual signals were assigned to indazolium cations, characterized by the absence of the downfield shifted singlet corresponding to the *N*1-proton in contrast to free 1*H*-indazol (see section 2.2.1). Consequently, the counterion exchange was repeated with the proposed patent mixture (MEK/EtOH 10:9) until full conversion was confirmed by ^{1}H NMR. Stirring in aqueous ethanol to dissolve intermixed CsBr afforded the required hydrate **2b** as dark purple microcrystalline solid in elemental analysis purity (62% yield, **Scheme 6**).

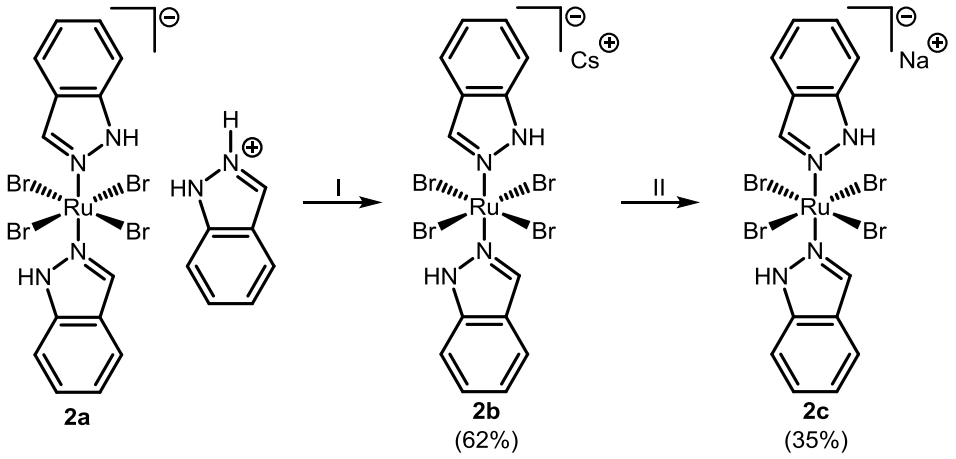

Scheme 6 Synthesis of **2b** and **2c**
(I) i) = CsBr (3.3 eq.), EtOH:MEK (3:1), T = r.t. t = 2 h; ii) = CsBr (2.8 eq.) MEK/EtOH (10:9), T = r.t., t = 4 h; (II) 1.1 M $NaAl(SO_4)_2$, CsBr (0.1 eq.) T = r.t., t = 24 h

Synthesis of the desired complex **2c** was conducted with a slightly modified work-up procedure as described in the literature.[89] Herein, compound **2b** was combined with 1.1 M $NaAl(SO_4)_2$ as sodium source and a minimum amount of CsBr (0.1 eq.) to seed the formation of water insoluble caesium aluminium sulfate (**Scheme 6**). The salt metathesis was performed in a heterogenous and highly concentrated reaction mixture to foster precipitation of $CsAl(SO_4)_2$. Variation of the molarity of $NaAl(SO_4)_2$ (0.8 M and 1.5 M) neither improved yield nor product purity. After extraction with acetone, the sodium complex was precipitated with MTBE. Filtration afforded **2c** as brown-purple granular solid in moderate yield (34%, overall yield: 20%). Although considerable efforts have been made to obtain **2c** as pure substance, elemental analysis revealed small amounts of 1*H*-indazole impurification (3.3 wt%). The sodium analogue exhibited substantially increased water solubility (> 2 mM in 1% DMSO) compared to **2a** (0.7 mM in 1% DMSO).

2.1.3 Synthesis of complex salt **3**

Establishing a synthetic route for the iodido-analogue **3** would open the possibility to perform *in vivo* experiments with ^{125}I radioisotope-labelled derivatives to monitor the stability and accumulation of the applied complex. In order to obtain compound 3, synthetic approaches similar to complex **2** were performed (**Scheme 7**, **Table 1**).

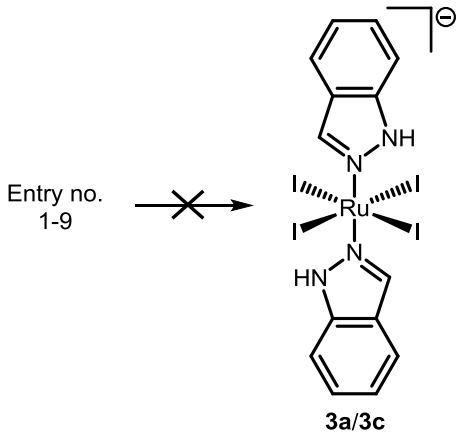

Scheme 7 Attempted synthesis of complex **3** (counterions are omitted for clarity)

Table 1 Applied conditions for the attempted synthesis of **3**[a]

Entry	Ru-source	I-source	Solvent	N-Donor
1	**1a**	KI	MeOH	HInd
2	**1a**	KI	EtOH	HInd
3	**1a**	KI	$CHCl_3/H_2O$ (1:1)	HInd
4	**1c**	NaI	EtOH	HInd
5	**1c**	NaI	H_2O	HInd
6[b]	**1c**	NaI	MeOH	HInd
7	RuI_3	HI	HI conc. (57%)	HInd
8[c]	RuI_3	HI	HI conc. (57%)	HInd
9[c]	RuI_3	HI	HI (28.5%)	HInd
10[c]	RuI_3	HI	HI conc. (57%)	HIm

[a]Conditions: T = 80 °C, t = 16 h. [b]Addition of $AgNO_3$. [c]RuI_3 generated *in situ*.

Heating to reflux of **1a** or **1c** in different solvents with iodide alkali salts lead to the formation of dark suspensions which contained a variety of not assignable species (entry 1-5). Activation of complex **1c** with $AgNO_3$ resulted in precipitation of the aqua-complex (entry 6), hence the focus was shifted towards utilization of RuI_3 as ruthenium source and HI as iodine source. RuI_3 was prepared according to literature procedure[94] by stirring a mixture of $RuCl_3.xH_2O$, KI and HI (57%) in water at room temperature. Subsequent purification with ethanol, followed by the addition of a mixture containing 1*H*-indazole dissolved in concentrated HI did not yield the desired product (entry 7). Repetition experiments were performed with *in situ* generated RuI_3 (prepared as described in section 2.1.2) in concentrated and half-concentrated hydroiodic acid (entry 8, 9). Unfortunately, the desired complex **3** could not be obtained.

It can be hypothesized that formation of the complex is prevented by steric collisions of the bulky iodido ligands, with 1*H*-indazole having a minor influence. The fact that replacement of the *N*-donor with steric less demanding 1*H*-imidazol (HIm) did not show any conversion as well strengthens this hypothesis (entry 10).

2.1.4 Synthesis of Rh(III) complex salt **4**

Preparation of the Rh(III)-based complex was performed utilizing procedures derived from the patent synthesis of BOLD-100.[89] Thus, $RhCl_3.xH_2O$ was converted to **4c** in a three step synthetic route as previously described in section 2.1.1. Optimized reaction conditions comprised application of a higher excess 1*H*-indazole (7.8 eq.) and prolonged reaction times for the first two steps.

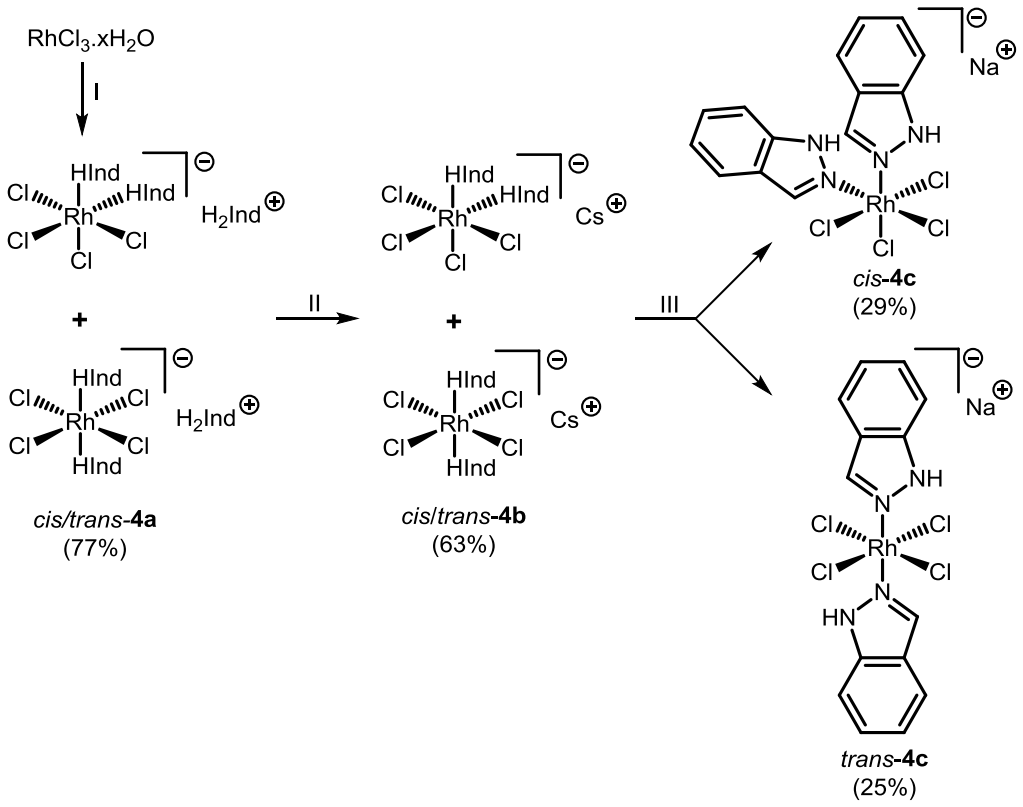

Scheme 8 Synthesis of complexes *cis*-**4c** and *trans*-**4c**
(I) i) = HCl conc., EtOH, T = reflux, t = 2 h; ii) = 1*H*-Ind (7.8 eq), HCl conc., T = 85° C, t = 16 h;
(II) i) = CsCl,(2.8 eq), MEK/EtOH (10:9), T = r.t., t = 2 h; ii) = EtOH/H_2O (2:1), T = r.t., t = 15 min;
(III) 1.1 M $NaAl(SO_4)_2$, T = r.t., t = 48 h

Notably, analysis *via* ^1H NMR revealed that both (H_2Ind) *cis*-$[RhCl_4(HInd)_2]$ and (H_2Ind) *trans*-$[RhCl_4(HInd)_2]$ are formed within the first step (**Scheme 8**). Separation of the isomers was achieved by fractional crystallization after conversion to the corresponding sodium analogues. The mixture of isomers was dissolved in acetonitrile, and addition of a small amount MTBE lead to precipitation of orange microcrystalline *trans*-**4c** (25% yield). Further addition of MTBE to the filtered solution yielded *cis*-**4c** as yellow fine-powdered material (29% yield). Examination of the filtered material after 2 h of reaction time in step I demonstrated that *trans*-**4a** was present predominantly, indicating that *trans*-**4a** is kinetically favoured, whereas *cis*-**4a** is the thermodynamic product. In contrast to **4a** and **4b**, the sodium complexes are water soluble.

2.1.5 Synthesis of complex salt **5**

In order to increase stability, replacement of the labile chlorido ligands by a suitable bidentate motif is a viable approach. The need for aquatic solubility and medium strong binding capabilities render oxalate as convenient choice. Furthermore, derivatization of cisplatin with bidentate carboxylate ligands culminated in the development of two worldwide approved anticancer drugs, *i.e.* carboplatin and oxaliplatin.

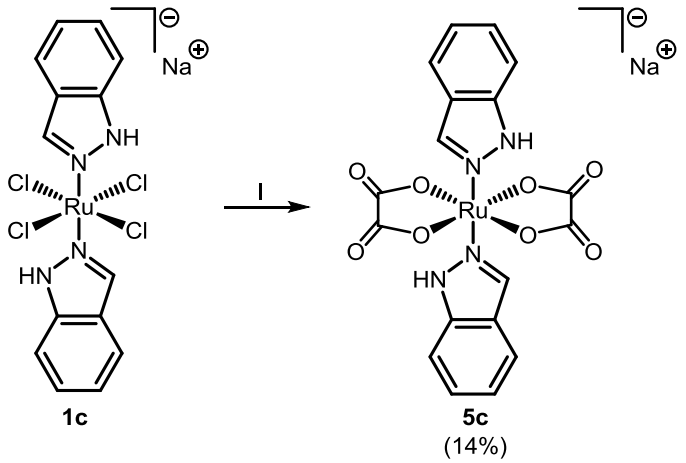

Scheme 9 Synthesis and proposed structure of complex **5c**
(I) silver oxalate (3.5 eq.), MeOH (dry), Schlenk technique, T = r.t., t = 48 h

Initial experiments conducted with **1a** and **1c** and sodium oxalate as bidentate ligand source showed no conversion. To our delight, reaction of **1c** with silver oxalate in dry MeOH led to the formation of complex **5c** (**Scheme 9**). After filtration, precipitation with diethyl ether afforded the desired compound as orange-red solid in poor yield (14%). However, conversion was not observed in acetone or acetonitrile, as confirmed by ESI-MS. Since precursor **1c** is employed as dihydrate, the low yield can be explained by formation and subsequent precipitation of the aqua species. A considerable amount of insoluble dark solid remained in the filter, which was attributed to the side product.

The water-soluble complex **5c** was dissolved in brine without inducing precipitation, indicating that no Ag(I) impurities are present in the isolated product. Furthermore, the paramagnetic nature of the complex was indirectly confirmed *via* ^{1}H NMR. Unfortunately, single crystals suitable for X-ray diffraction analysis could not be obtained, thus **Scheme 9** outlines a structural proposal.

2.1.6 Synthesis of complex **6**

Establishing a synthetic route for the incorporation of ligands featuring the general *O,O*-chelating 1,3-diketone-based core would open the possibility to introduce three additional derivatization sites (see **Figure 11**). Thus, linkage of targeting moieties would allow further fine-tuning of the anticancer properties. In addition, several Ru(II)-arene based complexes bearing acetylacetonato (acac) moieties with promising anticancer properties have been reported in the literature.[95,96]

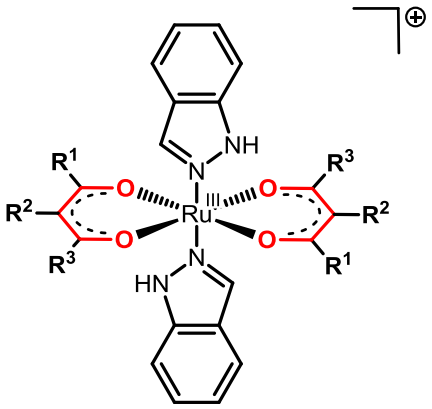

Figure 11 General structure of aimed complex featuring 1,3-diketone-based core (red) with possible derivatization sites R^1, R^2 and R^3

Preparation of **6** was conducted utilizing the previously synthesized complexes as precursors. To examine the influence of different leaving groups and counterions on the outcome of the reaction, compounds **1a**, **1c**, **2a**, **2b** and **2f** were employed. The general procedure involved deprotonation of the acac ligand with a suitable base, followed by addition of the respective precursor. Several approaches under different conditions were investigated (**Scheme 10**, **Table 2**).

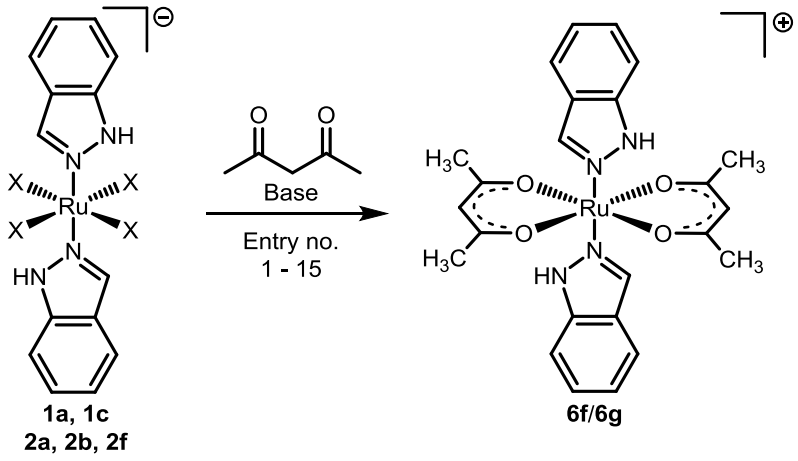

Scheme 10 Synthesis of complex **5** (counterions are omitted for clarity)

Table 2 Applied conditions in order to synthesize complex **5**[a]

Entry	Precursor	Base	Solvent	Product formation[b]
1	**1c**	Sodium acetate	H_2O	-
2	**1c**	NEt_3	MeOH	-
3	**1c**	NEt_3	EtOH	-
4[c]	**1c**	NEt_3	MeOH	-
5[d]	**2a**	NEt_3	MeOH	Yes
6[d]	**2a**	NEt_3	EtOH	Yes
7	**1c**	NEt_3	EtOH/H_2O (7:3)	Yes
8	**1a**	NEt_3	EtOH/H_2O (7:3)	-
9[e]	**2a**	NEt_3	EtOH/H_2O (7:3)	Yes
10[e]	**2b**	NEt_3	EtOH/H_2O (7:3)	Yes
11	**2f**	NEt_3	EtOH/H_2O (7:3)	-
12	**2a**	NEt_3	DCM	-
13	**2b**	NEt_3	Acetone	Yes
14	**2f**	NEt_3	Acetone	-
15[f]	**1c**	NaOMe	Acetone	Yes

[a]Conditions (unless noted otherwise): Precursor (1 eq), acac (2.2 eq.), T = r.t., t = overnight. [b]Confirmed *via* ESI-MS. [c]Addition of $AgNO_3$. [d]T = reflux. [e]acac (4.2 eq). [f]Inert atmosphere.

Application of water as solvent is not recommended due to rapid precipitation of the aqua complex under alkaline conditions (entry 1). Thus, weakly coordinating polar protic solvents such as methanol or ethanol employed with triethylamine as base appeared more suitable, but no conversion was observed with precursor **1c** (entries 2–4). Notably, bromido-analogue **2a** showed higher reactivity towards leaving group exchange (entries 5, 6) under these conditions. After stirring overnight, product formation was confirmed *via* ESI-MS. Depending on the employed precursor, solvent mixtures of EtOH/H_2O (7:3) afforded the desired complex as well, reflected by typical colour change to a bright blue solution (entries 7–11). However, compound mixtures containing inseparable side products were obtained (**Figure 12**). Purification by standard techniques such as column chromatography, extraction and fractional crystallization was not successful. Consequently, the reaction was conducted with **1c** in dry acetone and sodium methanolate as base, aiming for the formation of a single product and precipitation of resulting NaCl (entry 15). Unfortunately, the target compound could not be isolated. Although the foundation for the synthesis has been set, purification of the desired complex **6** needs to be established.

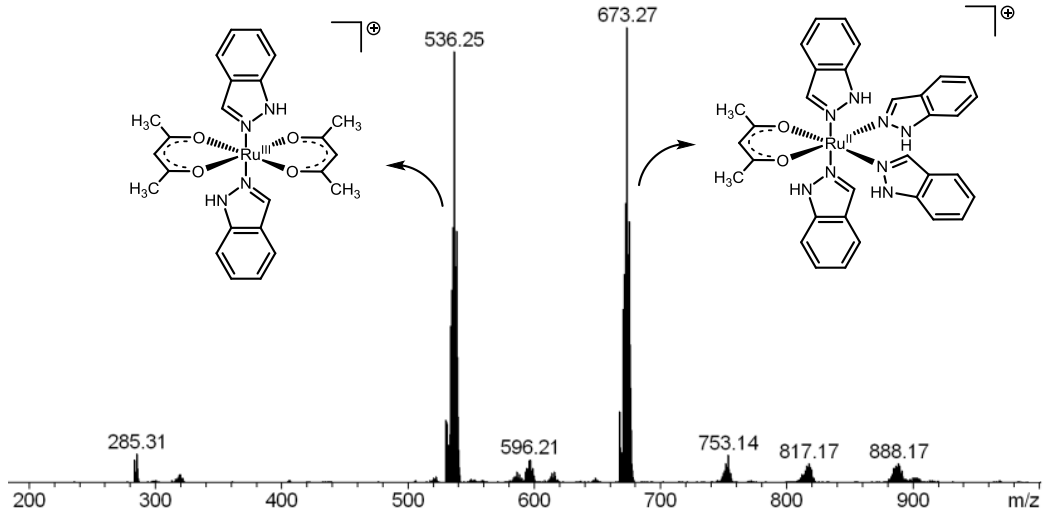

Figure 12 ESI-MS spectrum of entry 8 with desired product (left) and identified side product (right)

2.1.7 Synopsis of the synthesized complexes

The synthesized and isolated complexes featuring the lead structure of two *trans*-coordinated 1*H*-Indazole ligands to the metal core are outlined below (**Figure 13**). **4a** and **4b** were isolated as *cis*/*trans*-isomers and are therefore not included.

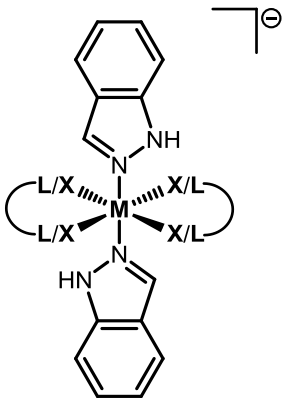

Complex	Metal	X/L	Counterion
2a	Ru	Br	H_2Ind^+
2b	Ru	Br	Cs^+
2c	Ru	Br	Na^+
2d	Ru	Br	$n\text{-}Bu_4N^+$
2e	Ru	Br	Ph_4P^+
trans-**4c**	Rh	Cl	Na^+
5c	Ru	ox	Na^+

Figure 13 Synthesized complexes in the course of this thesis sharing the same lead structure

2.2 Characterization

2.2.1 NMR spectroscopy

Characterization of the Ru-based complexes **2a–2e** and **5c** by NMR spectroscopy is difficult owing to the paramagnetic Ru(III) core. However, ^{1}H NMR proton signals of the bromido complex **2a** were partially resolved using different techniques: Recorded in DMSO-d_6, two upfield shifted broad singlets can be found at a δ = -8 and -14.5 ppm for the protons closest to the paramagnetic metal centre, and were thus assigned to H1 and H3 of the coordinated 1*H*-indazole. Upon addition of MeOH-d_4, the signal at -8 ppm disappeared due to rapid proton-deuterium exchange, hence confirming the labile proton at *N*1. The remaining signals were assigned in pairs *via* a COSY experiment at δ = 2.2 (2H, H4 or H7), 2.3 (2H, H4 or H7), 3.0 (2H, H5 or H6), and 3.29 (2H, H5 or H6) ppm. Accordingly, protons in a farther position from the paramagnetic centre can be found at more downfield shifts. Signals of the indazolium counterion were detected at the expected shift range except for H1. This signal is barely visible due to interactions with the paramagnetic complex (**Figure 14**).

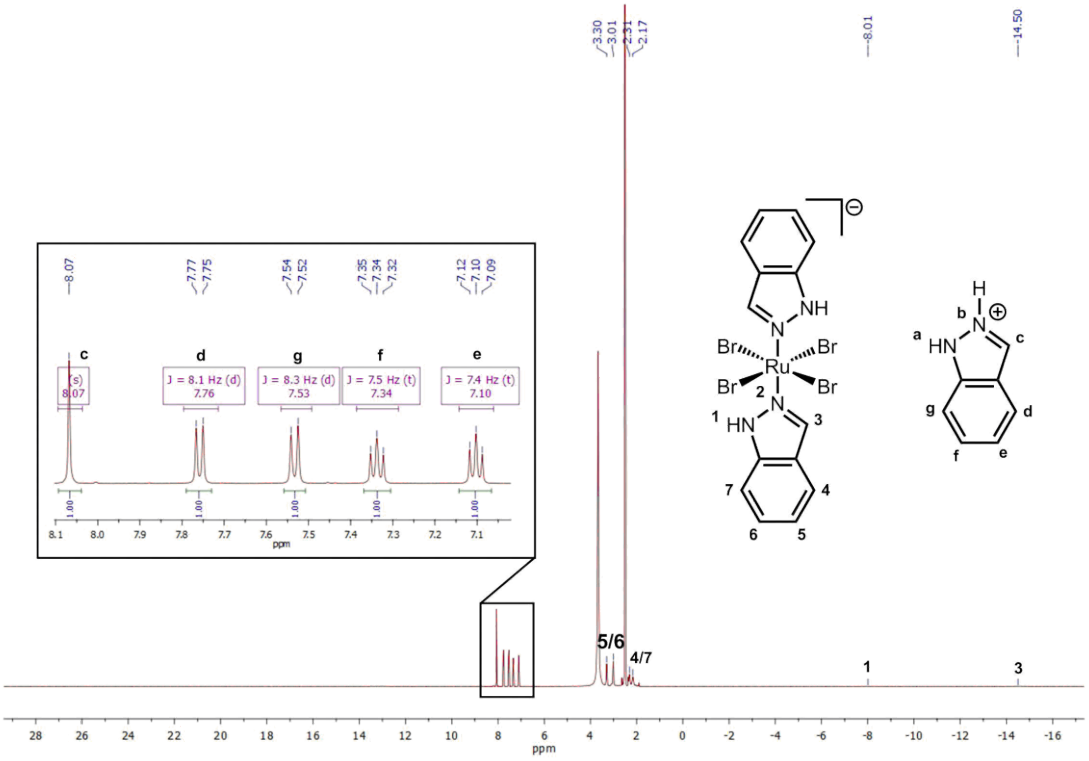

Figure 14 ^{1}H NMR spectrum of **2a** in DMSO-d_6

The use of NMR spectroscopy to determine and characterize the structure of a paramagnetic complex is extremely limited, thus other characterization methods were routinely applied (*vide infra*).

Rhodium-derived complexes **4** were characterized by means of ^{1}H, ^{13}C and 2D NMR in DMSO-d_6. The most prominent effect in ^{1}H NMR upon ligand coordination was observed for H3. Compared to free 1H-indazole, the signal was shifted downfield by approximately 0.4 ppm for *trans*-**4c** and 0.7 ppm for *cis*-**4c**, caused by electron withdrawing effects of the metal centre (**Figure 15**). Consequently, this transfer of electron density results in an upfield shift by 0.3 ppm of H1 which is then observed as sharp singlet. In contrast to H7, the remaining aromatic protons H4, H5 and H6 are far less exposed to deshielding effects induced by metal coordination. Exchange of the counterion showed no impact on the chemical shifts of the ligands.

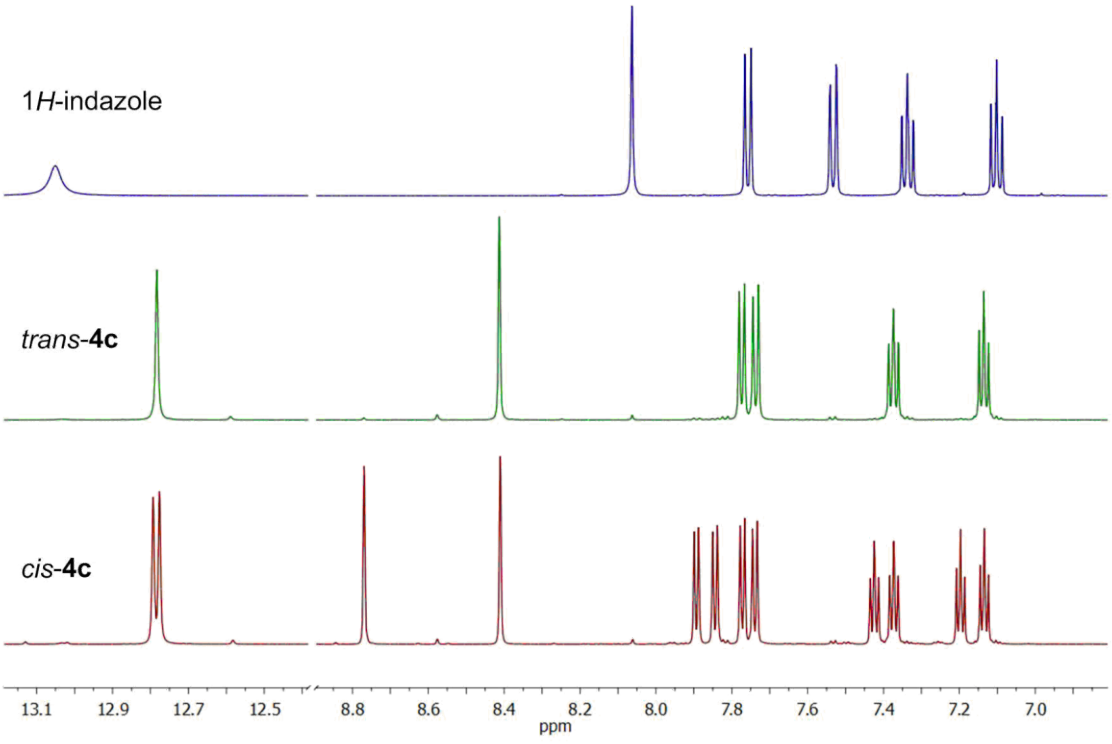

Figure 15 ^{1}H NMR spectra of 1*H*-indazole (top), *trans*-**4c** (mid) and *cis*-**4c** (bottom) in DMSO-d_6

2.2.2 ESI-mass spectrometry

Electrospray ionization induces a low degree of fragmentation and is therefore considered as soft ionization technique. This characteristic enables detection of non-covalent aggregates such as metal complexes. Thus, ESI-MS is a valuable method for the verification of complex formation, particularly for the obtained paramagnetic species.

Two characteristic peaks of the negatively charged complexes **2a–f**, **4a–c** and **5c** were typically observed, corresponding to the molecular anion [M-cation]$^-$ and the single negatively charged molecular anion without coordinating *N*-donor ligands $[RuX_4]^-$ or $[Ru(ox)_2]^-$ (**Figure 16**). The experimentally found isotope distribution patterns of the respective peaks are in accordance with theoretical calculations. Mass spectra recorded in the positive ion mode frequently resulted in intricate fragmentation patterns and were therefore less suited for product verification.

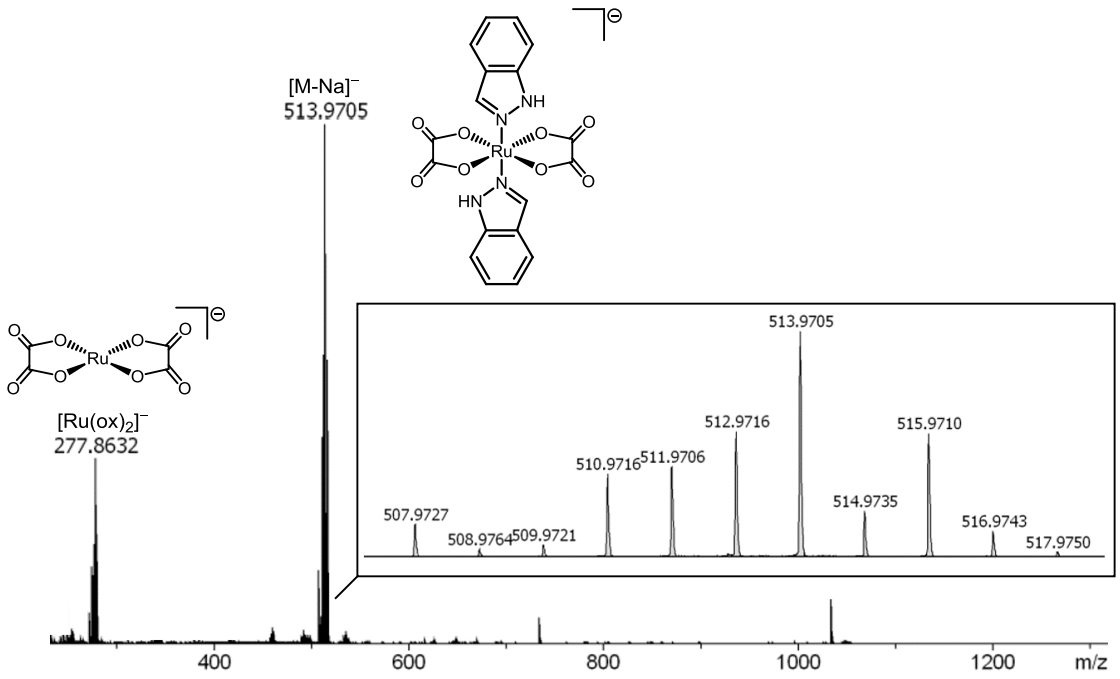

Figure 16 High resolution mass spectrum of **5c**, featuring the two characteristic peaks of [M-Na]$^-$ and $[Ru(ox)_2]^-$, the enlarged area represents the isotopic distribution pattern of the molecular anion

2.2.3 X-ray diffraction analysis

Crystallographic analysis is a powerful tool to determine the coordination motif of metal complexes, particularly for paramagnetic compounds. The structure of the complexes **2c**, **2e**, **2*** and *cis*-**4c** was unambiguously confirmed by X-ray diffraction analysis (**Figure 17**). Efforts to obtain crystals of **2a** resulted in the formation of **2*** due to rearrangement reactions (see section 2.1.2). Single crystals suitable for X-ray crystallography were obtained by liquid-liquid or vapour diffusion of appropriate solvents. The utilized technique and appropriate solvent systems are described in the experimental section. In addition, single crystals of the newly formed Ru(II) species **2$_{DMSO}$** (see section 2.4.1) were obtained and analyzed (**Figure 17**). Unfortunately, attempts to prepare single crystals of *trans*-**4c** and **5c** resulted in crystals of rather poor quality and were inapplicable to crystallographic analysis.

In all cases, the heterocyclic ligands are coordinated through the N2 nitrogen to the octahedral metal center. The *trans* configuration of the Ru-based complexes was confirmed, where the 1*H*-indazole ligands are located in the same plane. The bond angles of the prepared compounds are in the typical range for octahedral complexes. To compare the bond lengths of the different configurated complexes, the respective longest and shortest bonds were assessed (**Table 3**).

In general, M–Cl bond distances are considerably shorter than M–Br bonds. Compared to reported Ru(II)–halide bond lengths, the Ru(III)–X distances of the analyzed complexes are significantly shorter (*e.g.* Ru(II)–Cl: 2.409 Å, Ru(II)–Br: 2.538 Å).[56] These findings are in good agreement with the elongated Ru(II)-Br bond distance found in **2$_{DMSO}$**. Notably, bond lengths of the coordinated heterocycles to the Rh(III) center are substantially shorter compared to the Ru-derived complexes. As expected, counterion exchange had a minor impact on bond distances.

Table 3 Selected bond lengths of analyzed complexes

Bond length [Å]	**1e**[65]	**2c**	**2e**	**2$_{DMSO}$**	**2***	*cis*-**4c**
M–X$_{longest}$	2.372(8)	2.510(7)	2.499(8)	2.526(7)	2.484(6)	2.351(11)
M–X$_{shortest}$	2.359(8)	2.494(6)	2.489(5)	2.526(7)	2.477(7)	2.336(13)
M–N$_{longest}$	2.071(22)	2.071(5)	2.062(4)	2.092(8)	2.084(6)	2.018(11)
M–N$_{shortest}$	2.052(21)	2.071(5)	2.062(4)	2.092(8)	2.066(9)	2.008(11)

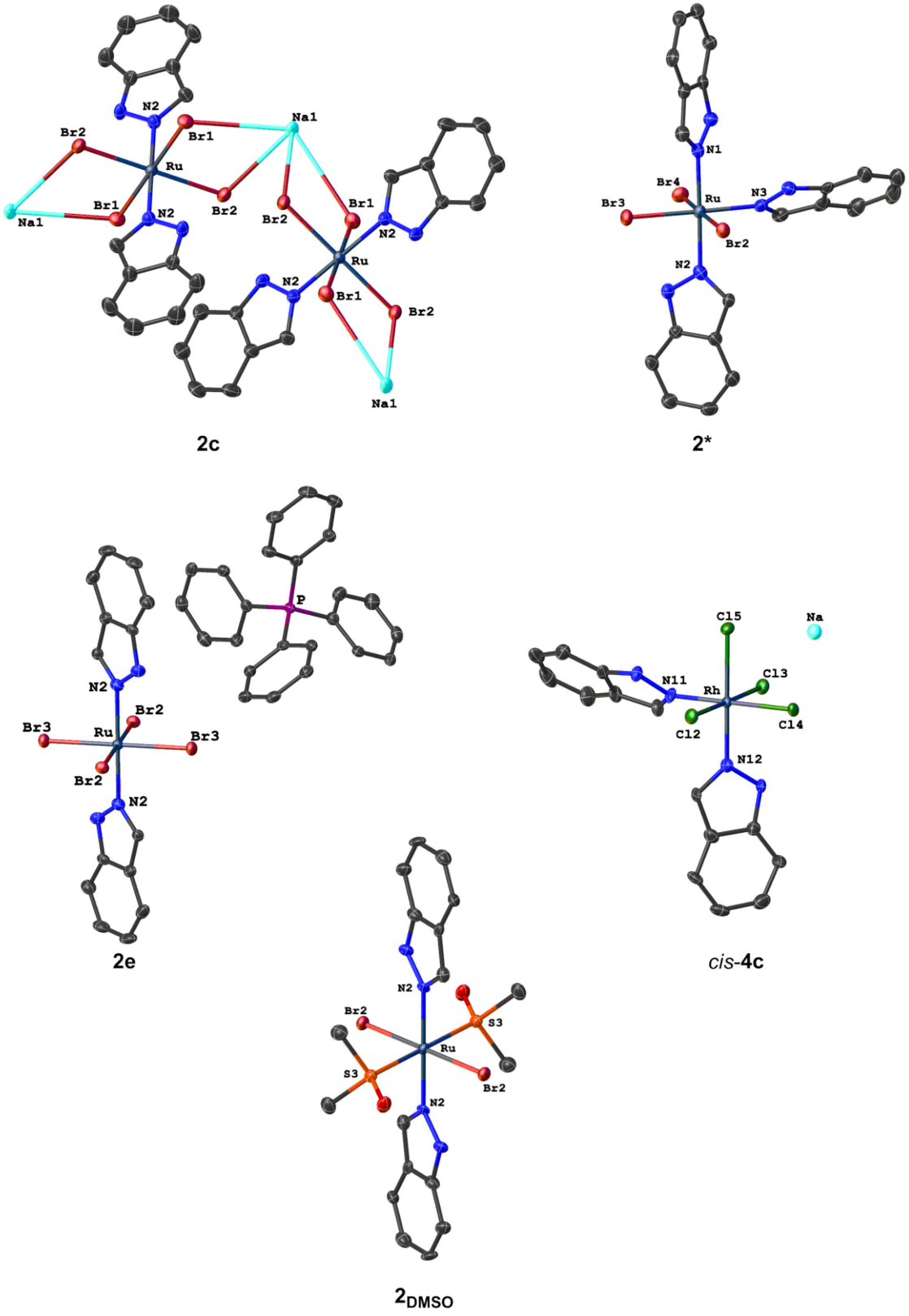

Figure 17 Crystal structure of complexes **2c**, **2***, **2e**, *cis*-**4c** and $\mathbf{2}_{\mathbf{DMSO}}$ (hydrogens are omitted for clarity)

2.3 Cyclovoltammetry

The electrochemical behavior of the novel complexes (**2a**, **2c**, *trans*-**4c** and **5c**) was investigated by cyclic voltammetry (CV) and compared to **1a** and **1c**. The cyclic voltammograms were recorded in DMSO (0.3 M [*n*-Bu_4N][BF_4]/DMSO) at a glassy carbon working electrode with a scan rate of 0.2 V s^{-1}.

In general, the different counterions had no influence on the redox behaviour of the complexes. As reported in the literature, complexes **1a** and **1c** feature an irreversible one-electron reduction wave (I^{red}) corresponding to the $Ru^{III} \rightarrow Ru^{II}$ process with an $E_{p/2}$ potential of −0.44 V *versus* NHE. The bromido complexes **2a** and **2c** exhibited similar electrochemical behaviour, however, a markedly increased $E_{p/2}$ potential of −0.27 V *versus* NHE was displayed **(Figure 18)**. These findings suggest *in vivo* reduction of complexes **2a** and **2c** to their more labile Ru^{II} counterpart proceeds faster compared to the chlorido analogues, which could impact the anticancer activity.

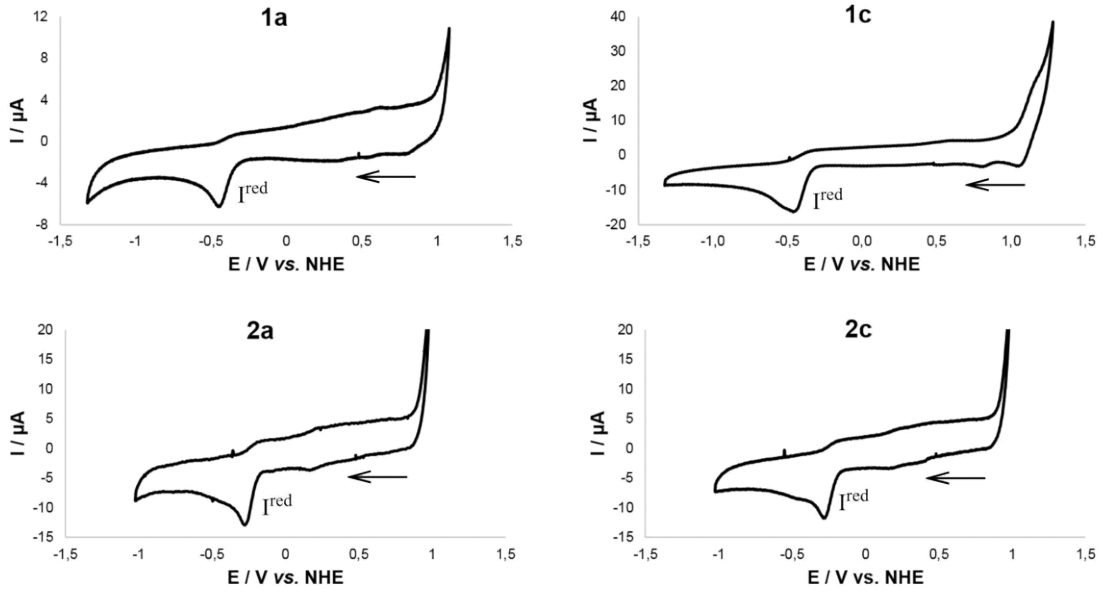

Figure 18 Cyclic voltammogramms of **1a**, **1c**, **2a** and **2c**

Rh-derived complex *trans*-**4c** shows more intricate electrochemical behaviour, with two consecutive irreversible reduction waves (a^{red} and I^{red}) with an $E_{p/2}$ potential of −0.88 V and −1.5 V *versus* NHE, respectively **(Figure 19)**. The reduction waves may be attributed to the $Rh^{III} \rightarrow Rh^{I}$ process, and an addition irreversible oxidation wave (a^{ox}) with an $E_{p/2}$ potential of 0.52 V *versus* NHE can be detected in the cyclic voltammogram. Further investigations are required to describe the occurring redox processes more precisely.

Notably, a reversible one-electron reduction wave attributed to the $Ru^{III} \longrightarrow Ru^{II}$ process is displayed in the cyclic voltammogram of complex **5c** (**Figure 19**), with an $E_{1/2}$ potential of −0.27 V *versus* NHE. The redox wave is characterized by a peak-to-peak separation (ΔE_p) of 50 mV and an anodic peak current (i_{pa}) that is almost equal to the cathodic peak current (i_{pc}), as required for reversible electron transfer processes. This reversible process can be attributed to the stabilizing effect of the chelate ligand. Thus, it can be hypothesized that oxalate bearing complex **5c** offers beneficial redox activity, which suggests further investigation of this promising compound. The obtained potentials of the Ru-based complexes are summarized below (**Table 4)**.

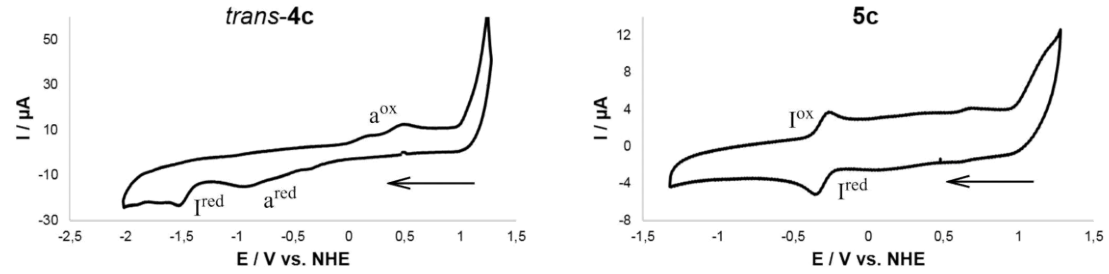

Figure 19 Cyclic voltammograms of *trans*-**4c** and **5c**

Table 4 Cyclic voltammetric data of the synthesized complexes

	1a*	**1c***	**2a***	**2c***	**5c**
$E_{1/2}{}^a$	−0.44	−0.44	−0.27	−0.27	−0.28

$^a E_{1/2}$ ($E_{1/2} = (E_{pa} + E_{pc})/2$) are given in V; $E_{p/2}$ for irreversible waves are indicated by an asterisk.

2.4 Stability studies

2.4.1 ^{1}H NMR

The stability in aqueous solutions of drug candidates is a key factor for further development.[97] Initial experiments to investigate the stability of the complexes were performed *via* ^{1}H NMR at 25 °C. To obtain comparable results, the *trans* isomer of **4c** was probed. Compounds **2a** and **2c** were examined in DMSO-d_6 due to rapid precipitation in aqueous solution, as reported for the chlorido complexes **1a** and **1c**.[98] In contrast, the Rh-derived complex *trans*-**4c** and oxalate bearing derivative **5c** were dissolved in D_2O. Repetitive scan spectra were recorded every hour for 24 h.

For *trans*-**4c** and **5c**, a decrease in intensity of the signals over 24 hours due to precipitation was observed. No new signals were detected, indicating the precipitation of a water-insoluble aqua species. However, the signals of *trans*-**4c** were still clearly visible after the measured timeframe, suggesting that formation of the aqua species is considerably slower compared to **1c** (**Figure 20**).

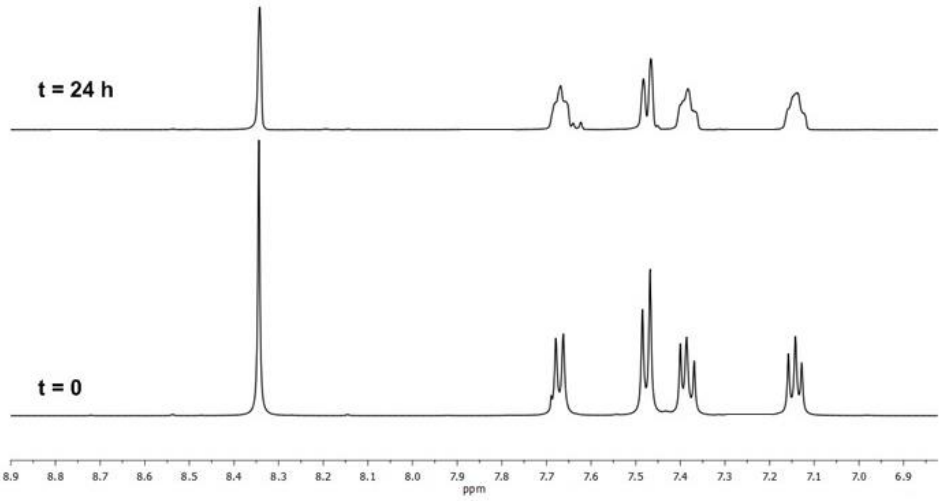

Figure 20 ^{1}H NMR of *trans*-**4c** in D_2O after 0 and 24 hours at 25 °C

Notably, pronounced solvolysis behaviour in DMSO-d_6 of the bromido complexes **2a** and **2c** was observed. After nine hours, sharp signals started to arise in the aromatic region which intensified substantially over time (**Figure 21**). The new signals featured the characteristic pattern of 1*H*-indazole, however, were shifted downfield compared to the free heterocycle.

These findings suggested the formation of a diamagnetic Ru(II)-species by reduction of the Ru(III) parent compound. No similar transformations were detected for **1a** and **1c** in the same timeframe.

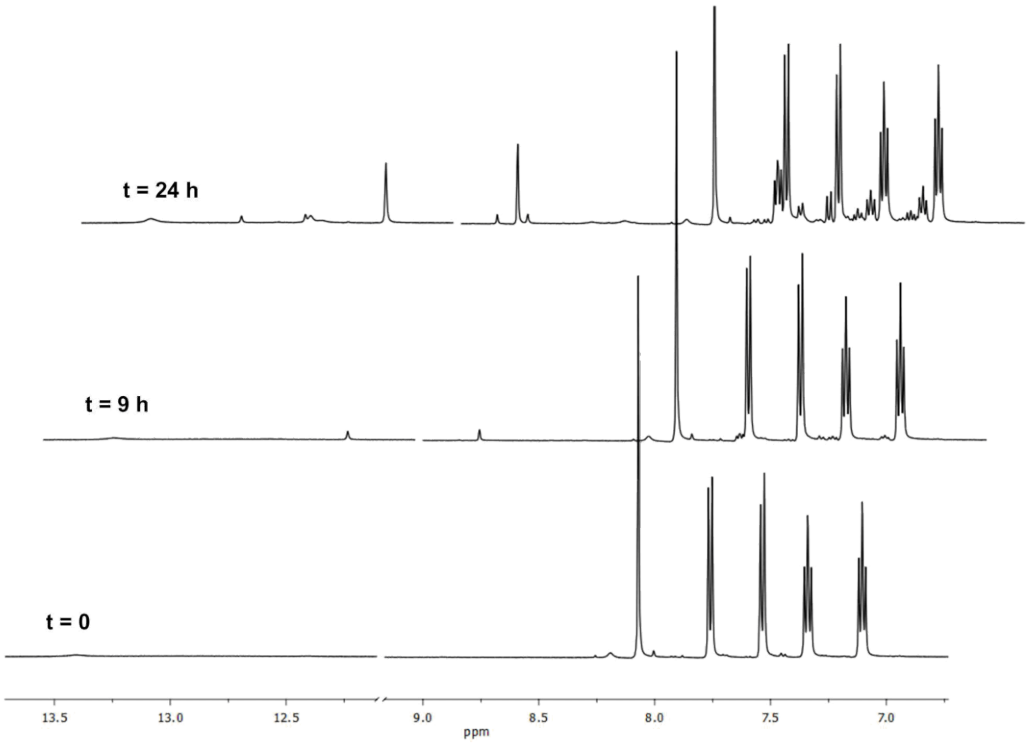

Figure 21 ^{1}H NMR of **2a** in DMSO-d_6 after 0, 9 and 24 hours at 25°C

After 4 days, single crystals suitable for X-ray diffraction precipitated from the solution. Crystallographic analysis confirmed the presence of coordinated 1*H*-indazole in the neutral *trans,trans,trans*-[$Ru^{II}Br_2(DMSO)_2(HInd)_2$] $\mathbf{2_{DMSO}}$ complex (**Scheme 11**). Intriguingly, the same product was obtained with **2b** and **2c** in repetition experiments, demonstrating that the counterion has no influence on the formation of the Ru(II)-species. The conversion presumably proceeds *via* reduction of the Ru(III)-center, followed by the replacement of the bromido groups by softer DMSO ligands.

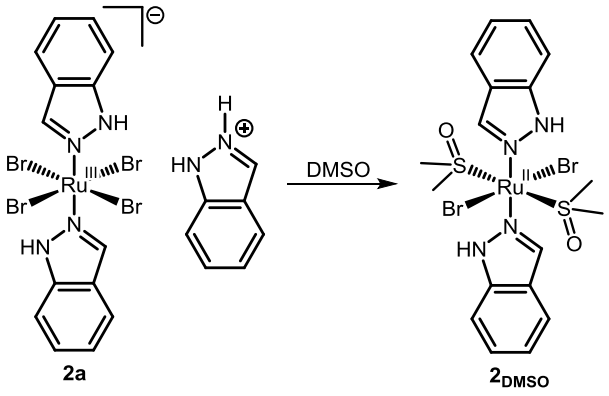

Scheme 11 Synthesis of $\mathbf{2_{DMSO}}$

2.4.2 UV–vis

UV–vis spectra of the developed complexes **2a**, **2c**, *trans*-**4c** and **5c** were recorded in aqueous solutions (50 µM, 1% DMSO) under different conditions and compared to the hydrolytic behaviour of **1a** and **1c**. Experiments were carried out at pH 7.4 (37 °C), reflecting the conditions in a healthy cell, and pH 6.0 (37 °C) as model system for the lower pH present in tumor cells due to hypoxia (see section 1.3).[99] In addition, measurements in citrate-buffered solutions at pH 3.4 (25°C) were carried out, as it is known from the formulation process that the parent compound **1c** exhibits excellent stability in this environment.[89] This in turn enables direct comparison of the stabilities of complexes **1a** and **1c** with the novel compounds. UV–vis spectra were collected at 30 minute intervals over 24 hours of incubation.

In general, the sodium or indazolium counterions had a minor influence on the appearance of the spectra (**Figure 22**). All Ru(III)-based complexes showed a characteristic band at ~290 nm, likely arising from ligand-to-metal charge transfers.[100] In the case of Rh(III)-based complex *trans*-**4c**, the corresponding peak is shifted hypsochromic and can be found at ~ 265 nm. These distinctive bands can be detected independently from pH and temperature. The fact that no formation of free 1*H*-indzaole (λ_{max} = 280 nm in aqueous solution)[101] was observed during the measured periods suggests that the heterocycles remain coordinated to the metal centers. Thus, decrease of signal intensity may be attributed to precipitation of the corresponding aqua complexes or formation of polynuclear hydroxo- or oxo-bridges species, respectively.[97]

As reported in the literature, the stability of the parent compounds **1a** and **1c** strongly depends on the pH value of the solution (**Figure 22**).[102] At a pH value of 3.4, the complex remains intact over 24 hours and no visible precipitation or colour change of the solution was observed. In contrast, extensive transformations were observed at higher pH values, resulting in slow precipitation of an insoluble species.

The band at 500 nm gives rise to the deep purple colour of the bromido analogues **2a** and **2c** (**Figure 22**). Furthermore, a characteristic shoulder can be found at 450 nm, both presumably arising from d–d transitions. Concerning the stability in aqueous solution, a markedly more susceptible behaviour towards aquation was observed. Whereas chlorido bearing complexes **1a** and **1c** remained unaffected at pH = 3.4, **2a** and **2c** showed decomposition over 24 hours, with isosbestic points at 325 nm and 385 nm.

Notably, the absorption bands at 450 nm and 500 nm diminished within minutes at pH = 6. The intensity of the signals of **2a** and **2c** decreased continuously over time, which can be attributed to precipitation of the aquation product. The most pronounced effect was observed at physiological pH, where almost quantitative precipitation occurred after 24 hours of incubation.

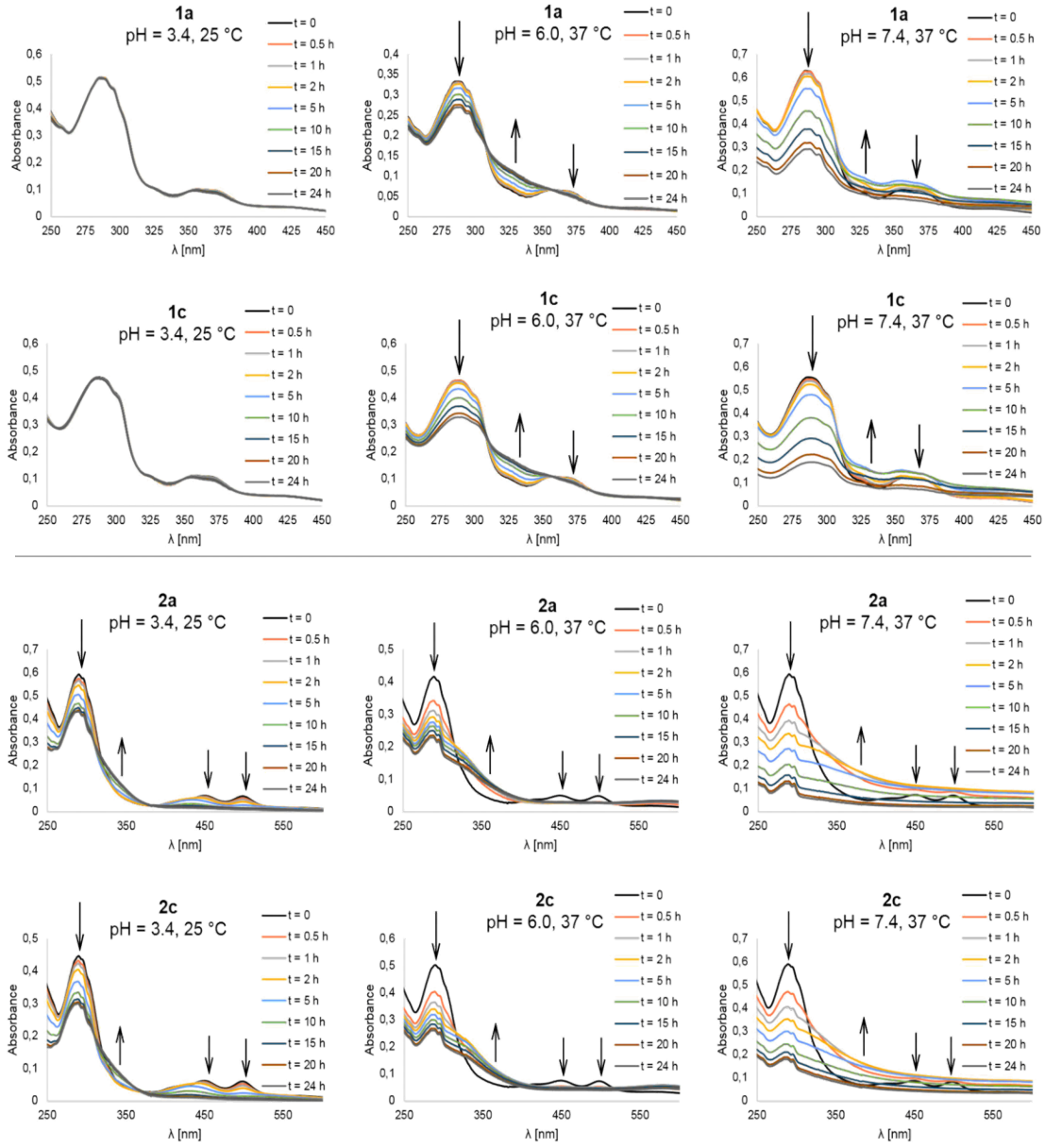

Figure 22 UV–vis spectra of **1a**, **1c**, **2a** and **2c** recorded in citrate buffered (pH = 3.4, 25°C), phosphate buffered (pH = 6.0, 37 °C) and PBS buffered (pH = 7.4, 37 °C) solutions

In contrast, complex *trans*-**4c** exhibited remarkable hydrolytic stability at acidic pH values (**Figure 23**). Merely incubation in alkaline solution led to slow decomposition of the complex, showing an isosbestic point at 280 nm in the UV-vis spectrum. Complex **5c** exhibited rather pH independent hydrolytic behavior, however, decomposition was pronounced under physiological pH value (**Figure 23**). The corresponding spectra show isosbestic points at 310 nm, 380 nm (pH = 3.4) and 400 nm (pH = 6 and 7.4). No precipitation of the complex or aquation products was observed. Intriguingly, the chlorido bearing complexes were more stable at pH = 3.4 than **5c**, despite bearing a bidentate motif. Consistent with previous ^{1}H NMR investigations, it can be assumed that the oxalato ligands remain as leaving groups since no signals of uncoordinated 1*H*-indazole were detected in the spectra.

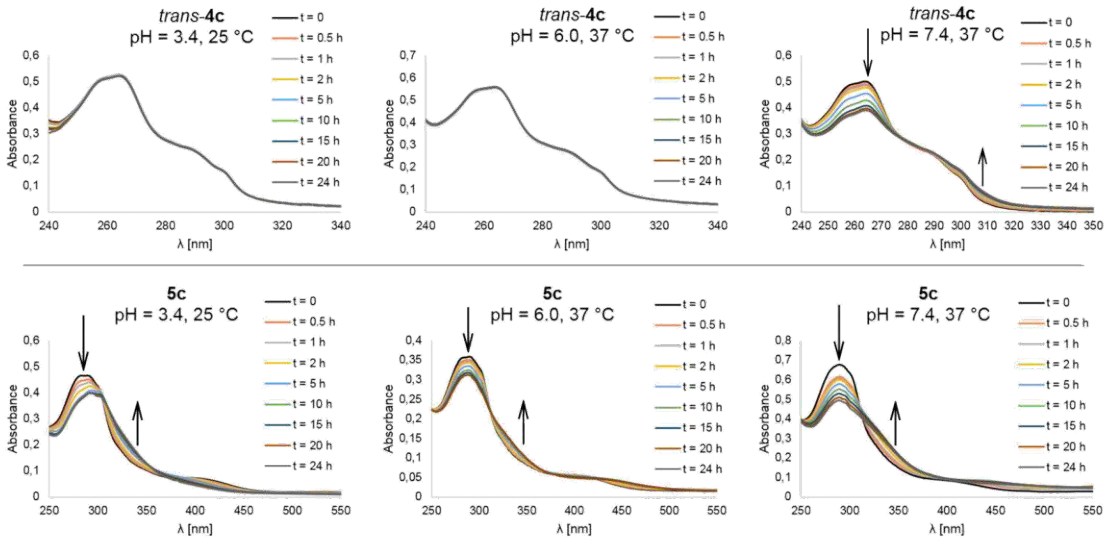

Figure 23 UV–vis spectra of *trans*-**4c** and **5c** recorded in citrate buffered (pH = 3.4, 25°C), phosphate buffered (pH = 6.0, 37 °C) and PBS buffered (pH = 7.4, 37 °C) solutions

To summarize, pH-dependent stability in aqueous solutions was observed, and the stability of the complexes can be ranked in the following order: *trans*-**4c**>**5c**>**1a**~**1c**>>**2a**~**2c**. Although the bromido complexes exhibit an almost identical $E_{1/2}$ potential as the oxalate complex **5c**, their stability in aqueous solution differs markedly. The different observed behaviors of the novel complexes compared to their parent compounds **1a** and **1c** strongly suggest *in vitro* evaluation of their anticancer properties.

3 Conclusion and Outlook

Modification of the leaving groups and the metal center of the first-in-class Ru(III) drug candidate BOLD-100 has been examined. Over the course of this thesis, seven novel Ru(III)- and Rh(III)-based complexes featuring *trans*-coordinated 1*H*-indazole ligands were synthesized in good to moderate yields. Herein, monodentate and bidentate ligands were utilized and the water solubility of the complexes was substantially improved by counterion exchange. The novel compounds were characterized by standard analytical methods such as NMR spectroscopy, mass spectrometry and elemental analysis. Crystal structures of three complexes and two solvolysis products were obtained and allowed unambiguous confirmation of the coordination motifs. In contrast, attempts to synthesize iodido analogues of the lead compound were unsuccessful, presumably due to steric collisions. Furthermore, the synthetic foundations to insert highly versatile bidentate acac ligands have been set, however, purification needs to be established.

Studies on the electrochemical behavior of the complexes by cyclovoltammetry showed the impact of different leaving groups and the metal center. Exchange of the chlorido groups with bromido ligands led to a positive shift of the reduction potential, while variation of the metal center to rhodium resulted in a markedly distinct behavior. Notably, oxalato bearing complex **5c** displayed a reversible one-electron reduction wave which demonstrates the influence of chelate ligands on the redox properties.

Investigations of the complexes in aqueous solutions by means of UV-vis spectroscopy further revealed the significance of the nature of the leaving groups or the metal center on hydrolytic stability. While the bromido analogues were prone to hydrolysis under the studied conditions, the rhodium-derived complex *trans*-**4c** exhibited remarkable stability compared to the parent compound. Moreover, complex **5c** showed rather pH and temperature independent hydrolytic behaviour and reasonable overall stability.

The results presented within this work strongly suggest *in vitro* evaluation of the anticancer activities of the synthesized complexes. Furthermore, the possibility to introduce other bidentate motifs opens new perspectives for future development of novel derivatives. In essence, this work demonstrates that modification of the leaving group and/or metal center is a valuable approach to fine-tune the physicochemical properties of a lead structure.

4 Experimental Section

4.1 Materials and Methods

All solvents and chemicals were obtained by commercial suppliers and used without further purification, if not specified otherwise. Methanol, ethanol and acetone were distilled and dried over molecular sieve (3 Å) prior to use. Several compounds and reactions required inert atmosphere which was carried out under argon. For syntheses, the following chemicals and solvents were used: Ruthenium(III) chloride (Johnson Matthey), rhodium(III) chloride (Johnson Matthey), caesium chloride (Acros), caesium bromide (TCI), sodium sulfate (Sigma), $Al_2(SO_4)_3.18H_2O$ (Acros), hydrochloric acid (37%, Sigma), hydrobromic acid (48%, Sigma), 1*H*-indazole (Polivalent-95), sodium oxalate (Sigma), silver nitrate (Acros), molecular sieve (3 Å, beads, 4–8 mesh), tetra(*n*-butyl)ammoniumbromide (Sigma), tetraphenylphosphoniumbromide (Sigma).

NMR-spectroscopic experiments were performed at 25 °C on *Bruker Avance III*™ (500 and 600 MHz) and *Bruker Avance III*™ *HD* (700 MHz) FT-NMR spectrometer instruments. ^1H, ^{13}C and 2D NMR spectra were recorded in DMSO-d_6, MeOH-d_4 or D_2O. Chemical shifts (δ in ppm) are indicated relative to TMS and were referenced to residual protons in the solvent.[103] For stability investigations, samples were dissolved in DMSO-d_6 or D_2O and spectra were recorded in 60 minute intervals over 24 hours. To assign NMR signals, the numbering scheme below was utilized (**Figure 24**).

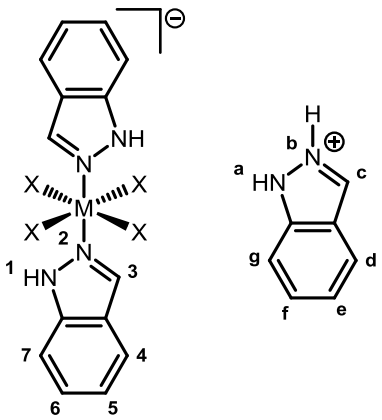

Figure 24 ^1H NMR signal assignment

ESI-MS spectra were recorded at the Core Facility for Mass Spectrometry of the University of Vienna (Faculty for Chemistry). Mass spectra were acquired in positive or negative ion mode on the following instruments:

- ESI-Qq-TOF mass spectrometer - *maXis UHR-TOF* (Bruker Daltonik GmbH, Bremen, Germany). Samples were injected *via* direct infusion in ACN/MeOH (1:1) +1% H_2O at a concentration of 5 µM with a flow rate of 3µL/min. Data files were processed using Bruker data analysis software *Compass 1.5* (version 3.2) and *DataAnalysis* (version 4.1). Spectra were recorded under the following conditions: Capillary voltage: -/+ 4500 V, dry gas flow: 4.0 L/min (Nitrogen), dry temperature: 180°C, mass range: 50-1900 m/z.
- ESI-3D ion trap mass spectrometer - *amaZon speed ETD* (Bruker Daltonik GmbH, Bremen, Germany). Samples were injected *via* direct infusion in ACN/MeOH (1:1) +1% H_2O at a concentration of 5 µM with a flow rate of 5 µL/Min. Data files were processed using Bruker data analysis software *ESI compass 1.4 for amaZon* (version 7.1) and *DataAnalysis* (version 4.0 SP 5). Spectra were recorded under the following conditions: Capillary voltage: -/+ 4500 V, dry gas flow: 5.0 L/min (Nitrogen), dry Temperature: 180°C, mass range: 50-3000 m/z.
- ESI-3D ion trap mass spectrometer - *HCT plus* (Bruker Daltonik GmbH, Bremen, Germany). Samples were injected *via HPLC Agilent 1100* in ACN/MeOH (1:1) +1% H_2O with a flow rate of 0.07 mL/min. Data files were processed using *Bruker Daltonics esquire 5.4* and *DataAnalysis* (version 3.3). Spectra were recorded under the following conditions: Capillary voltage: -/+ 3500 V, dry gas flow: 5.0 L/min (Nitrogen), dry temperature: 250°C, mass range: 50-3000 m/z.

Elemental analyses were performed at the Microanalytical Laboratory of the University of Vienna, using a *Perkin Elmer 2400 Series II CHNS/O Elemental Analyzer.*

X-ray diffraction analysis was carried out on *a Bruker X8 APEX2* diffractometer equipped with a multilayer monochromator and a Mo K/α *INCOATEC* microfocus sealed tube (λ = 0.71073 Å) spectrometer at 100 K and *Kryoflex* cooling devices.

Stability investigations in aqueous solution by **UV-vis spectroscopy,** spectra were recorded in 30 min intervals for 24 hours on a *Perkin Elmer Lambda 35* UV-vis spectrophotometer with a *PTP 6* (Peltier Temperature Programmer), and *Julabo AWC 100* recirculating cooler. Stock solutions (10 mM) of complexes were prepared in DMSO and diluted with the corresponding buffer to a concentration of 25 µM in 1% DMSO. Buffers at pH 7.4 (PBS, measured at 37 °C), 6.0 (phosphate-buffered, measured at 37 °C) and 3.4 (citrate buffered, measured at 25 °C) were employed to ensure a constant pH value. Buffers were prepared according to ref.[104]

Cyclic voltammograms were measured in a three-electrode setup using a 2 mm diameter glassy carbon working electrode, a platinum auxiliary electrode and an $Ag|Ag^+$ reference electrode containing 0.1 M $AgNO_3$. Experiments were performed at room temperature using an *EG & G PARC potentiostat/galvanostat A 273*. Solutions were degassed prior to measurements by passing a stream of argon through the solution for 5 minutes, and measurements were conducted under inert atmosphere. The potentials were acquired in a freshly prepared solution of 3 mL DMSO containing 0.3 M [*n*-Bu_4N][BF_4] using [Fe(η^5-C_5H_5)$_2$] ($E_{1/2}$ = 0.68 V *vs.* NHE)[105] as internal standard and are quoted relative to the normal hydrogen electrode (NHE).

The **solubility** of the compounds was determined in distilled H_2O containing 1% DMSO. The complexes were dissolved in DMSO and diluted with H_2O to an overall concentration of 1% DMSO. The stated solubility refers to the analyte concentration at which no precipitation was observed.

4.2 General procedures

The general procedures described below are adapted from the original patent procedure.[89] Utilized quantities and reaction times depend on the complex and are stated in the respective synthetic procedure. Exact compliance with the quantity specifications is recommended.

4.2.1 General procedure for the purification of MX_3 (MX_3 = $RuCl_3$, $RuBr_3$, $RhCl_3$)

Purification of $RuCl_3$, $RhCl_3$ and *in situ* generated $RuBr_3$ was carried out in a similar manner and is thus described for the following example. For $RuBr_3$, concentrated HBr was employed instead of conc. HCl.

Hydrated $RuCl_3$ (200 mg, 0.76 mmol) was dissolved in a mixture containing pure non-denatured ethanol (99%)/HCl conc. (10 mL, 1:1, v/v) and was heated to 90 °C for 30 minutes, followed by distillation under air at normal pressure until the mixture was reduced to one third of its original volume. The concentrated dark red ruthenium solution was subsequently filtered, and the filter was rinsed with 2 mL concentrated HCl. The combined filtrates were collected and contained exclusively Ru(III) chloride.

4.2.2 General procedure for the preparation of complex salts of the general formula $H_2Ind[MX_4(HInd)_2]$ (M = Ru, X = Cl, Br; M = Rh, X = Cl)

The described procedure refers to the respective halide X of the desired complex. An excess of 1*H*-indazole (6.6–8.0 eq.) was dissolved in concentrated HX and heated to 70 °C and stirred until all solids were completely dissolved. The concentrated and purified MX_3 solution (*vide infra*) was added dropwise to the stirred mixture, the flask was rinsed with a minimum amount of HX and added to the solution. Subsequently, the resulting solution was heated to 85 °C for several hours (10–16 h). Afterwards, the formed precipitate was filtered, the reaction flask rinsed with 2 M HX and added to the material on the filter. The filtered solids were thoroughly washed with 2 M HX and partially dried by suction for 6 hours. The crude and wet product, containing residual HX, was employed without further purification for the subsequent counterion exchange reactions.

To isolate the respective indazolium complex salt, the crude product was stirred in H_2O for two hours to remove HX residues. The solids were filtered and dried *in vacuo* to afford the desired indazolium complex as solid material.

4.2.3 General procedure for the preparation of complex salts of the general formula $Cs[MX_4(HInd)_2]$ (M = Ru, X = Cl, Br; M = Rh, X = Cl)

The described procedure refers to the respective halide X of the desired complex. The previously obtained crude indazolium complex salt (*vide supra*) was mixed with fine powdered CsX (2.8 eq.) in a beaker of appropriate size and combined with a mixture containing MEK and pure non-denatured ethanol 99% (10:9, v/v). The resulting heterogenous mixture was stirred for several hours (2–16 h) at room temperature. Afterwards, the solids were collected by filtration, the filtered material thoroughly washed with ethanol 99% and dried by suction. The obtained solvate was subsequently stirred in a mixture containing ethanol 99%/H_2O (2:1, v/v) for 15 minutes at room temperature, separated by filtration and washed thoroughly with ethanol 99%. The material was dried by suction, followed by drying *in vacuo* to provide the desired caesium complex.

4.2.4 General procedure for the preparation of complex salts of the general formula $Na[MX_4(HInd)_2]$ (M = Ru, X = Cl, Br; M = Rh, X = Cl)

A 1.1 M solution of $NaAl(SO_4)_2$ was prepared by gradually adding solid $Al_2(SO_4)_3.18H_2O$ (36.64 g, 55 mmol) in 80 mL H_2O, followed by the addition of Na_2SO_4 (7.81 g, 55 mmol). The resulting mixture was stirred until all solids were completely dissolved, and the total volume was diluted to 100 mL with H_2O. The solution was filtered prior to use.

The described procedure refers to the respective halide X of the desired complex. The prepared 1.1 M $NaAl(SO_4)_2$ solution was combined with the previously obtained caesium complex salt (*vide supra*) in a beaker of appropriate size. Fine powdered CsX (0.1 eq.) was added to the heterogenous mixture and the resulting slurry was stirred for several hours (24–48 h) at room temperature. Afterwards, the solids were collected by filtration and washed with saturated aqueous $Na_2(SO_4)$ in three portions. The obtained material was thoroughly dried *in vacuo*. The dried solids were stirred in acetonitrile for 15 minutes and the insoluble salts were separated by filtration. The salt cake was washed with acetonitrile until colourless. Subsequently, MTBE was added to the combined filtrates while stirring, and the flask was stored at 4 °C for one hour to complete the precipitation. The precipitates were collected by filtration, washed thoroughly with MTBE and dried *in vacuo* to afford the desired sodium complex.

4.3 Syntheses

4.3.1 Synthesis of Indazolium (*OC*-6-11)-tetrachloridobis(1*H*-indazole)ruthenate(III) (**1a**)

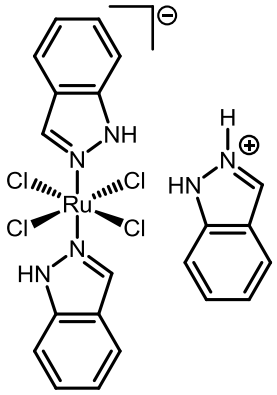

$C_{21}H_{19}Cl_4N_6Ru$
M = 598.30 g/mol

The synthesis was performed according to the general procedures described in sections 4.2.1 and 4.2.2, using $RuCl_3.xH_2O$ (200 mg, 0.76 mmol, 1.0 eq.) dissolved in 10 mL EtOH/HCl conc. and 1*H*-indazole (600 mg, 5.08 mmol, 6.6 eq.) dissolved in 5 mL concentrated HCl. After 10 hours of reaction time, the complex was stirred in 150 mL H_2O and isolated by filtration.

Yield: 420 mg (92%), ochre-coloured solid.

ESI-MS$^-$ *m/z* Found (Calculated): $[M–H_2Ind]^-$ 475.89 (475.88), $[RuCl_4]^-$ 243.78 (243.77).

^{1}H NMR (500.10 MHz, DMSO-d_6): δ(cation) = 8.06 (s, 1H, H_c), 7.75 (d, $^3J_{H,H}$ = 8 Hz, 1H, H_d), 7.52 (d, $^3J_{H,H}$ = 8 Hz, 1H, H_g), 7.33 (dd, $^3J_{H,H}$ = 7 Hz, $^3J_{H,H}$ = 7 Hz, 1H, H_f), 7.09 (dd, $^3J_{H,H}$ = 7 Hz, $^3J_{H,H}$ = 7 Hz, 1H, H_e) ppm; δ(anion) = 4.42 (bs, 4H, H_5/H_6), 3.27 (bs, 4H, H_4/H_7), -6 (bs, 2H, H_1), -11 (bs, 2H, H_3) ppm.

Elemental analysis:

$C_{21}H_{19}Cl_4N_6Ru \cdot 0.05\ H_2O \cdot 0.25$ HCl	C [wt%]	H [wt%]	N [wt%]	O [wt%]
Calculated	41.46	3.21	13.82	0.38
Found	41.72	2.95	13.79	0.13
Δ	0.26	0.26	0.03	0.25

4.3.2 Synthesis of Caesium (*OC*-6-11)-tetrachloridobis(1*H*-indazole)ruthenate(III) (**1b**)

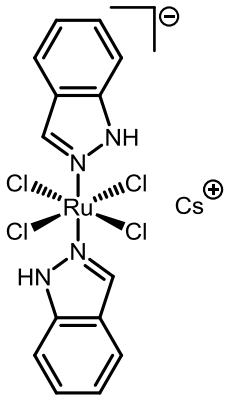

$C_{14}H_{12}Cl_4CsN_4Ru$
M = 612.05 g/mol

The synthesis was performed according to the general procedure described in section 4.2.3, using crude **1a** (1140 mg), CsCl (361 mg, 2.14 mmol, 2.8 eq.), a mixture of MEK (4 mL) and EtOH (3.6 mL) and a reaction time of 2 hours to form the solvate, a mixture of 2 mL EtOH with 1 mL H_2O and a reaction time of 15 minutes to form the hydrate. The equivalents of CsCl and the yield are calculated from employed $RuCl_3.xH_2O$ (200 mg, 0.76 mmol, 1.0 eq., calculated as $RuCl_3 \cdot 3H_2O$).

Yield: 468 mg (85%), red-brown microcrystalline solid.

ESI-MS$^-$ *m/z* Found (Calculated): $[M-Cs]^-$ 475.89 (475.88), $[RuCl_4]^-$ 243.78 (243.77).

^{1}H NMR (500.10 MHz, DMSO-d_6): δ(anion) = 4.42 (bs, 4H, H_5/H_6), 3.27 (bs, 4H, H_4/H_7), -6 (bs, 2H, H_1), -11 (bs, 2H, H_3) ppm.

4.3.3 Synthesis of Sodium (*OC*-6-11)-tetrachloridobis(1*H*-indazole)ruthenate(III) (**1c**)

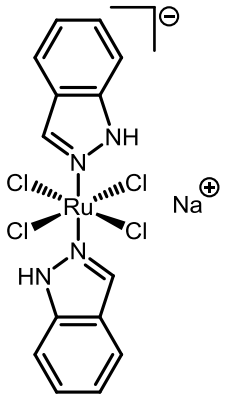

$C_{14}H_{12}Cl_4N_4NaRu$
M = 502.14 g/mol

The synthesis was performed according to the general procedure described in section 4.2.4, using **1b** (468 mg, 0.76 mmol, 1.0 eq.), 5.9 mL 1.1 M $NaAl(SO_4)_2$, CsCl (13 mg, 0.07 mmol, 0.1 eq.) and a reaction time of 30 hours. Afterwards, 9 mL sat. Na_2SO_4 were used for washing, 5 mL acetonitrile for the extraction and 18 mL MTBE for the precipitation.

Yield: 318 mg (83 %), voluminous brown powder.

ESI-MS$^-$ *m/z* Found (Calculated): $[M–Na]^-$ 475.88 (475.88), $[RuCl_4]^-$ 243.77 (243.77).

^{1}H NMR (500.10 MHz, DMSO-d_6): δ(anion) = 4.42 (bs, 4H, H_5/H_6), 3.27 (bs, 4H, H_4/H_7), -6 (bs, 2H, H_1), -11 (bs, 2H, H_3) ppm.

Elemental analysis:

$C_{14}H_{12}Cl_4N_4NaRu \cdot 1.5\ H_2O$	C [wt%]	H [wt%]	N [wt%]	O [wt%]
Calculated	31.78	2.86	10.59	4.54
Found	31.77	2.81	10.63	4.51
Δ	0.01	0.05	0.04	0.03

4.3.4 Synthesis of Indazolium (*OC*-6-11)-tetrabromidobis(1*H*-indazole)ruthenate(III) (**2a**)

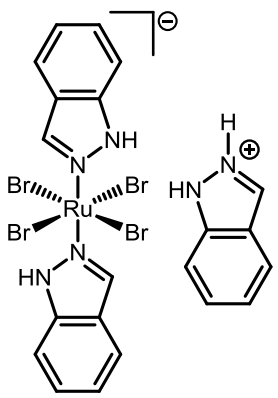

$C_{21}H_{19}Br_4N_6Ru$
M = 776.11 g/mol

Synthesis of *in situ* generated $RuBr_3$ was conducted as reported in the literature[91] with slight adaptations. $RuCl_3 \cdot xH_2O$ (150 mg, 0.57 mmol, 1.0 eq.) was dissolved in H_2O (4 mL), 10 M NaOH (200 µL) was added to the stirred solution and the resulting mixture heated to reflux for 20 minutes. Black $RuO_2 \cdot yH_2O$ (140 mg) was separated by filtration and thoroughly washed with H_2O and acetone. After drying *in vacuo*, $RuO_2 \cdot yH_2O$ was dissolved in 3 mL concentrated HBr at 0 °C for 1 hour. The dark solution was filtered, combined with a mixture of 3 mL HBr conc. and 3 mL EtOH and purified as described in section 4.2.1.

Subsequent preparation of the indazolium complex salt **2a** was performed according to the general procedure described in section 4.2.2, using 1*H*-indazole (542 mg, 4.59 mmol, 8.0 eq.). After 16 hours of reaction time, the complex was stirred in 130 mL H_2O and isolated by filtration. Attempts to grow single crystals by slow diffusion of *n*-hexane into an acetone complex solution resulted in the formation of crystalline **2***.

Yield: 523 mg (93%), purple solid.

ESI-MS$^-$ *m/z* Found (Calculated): $[M–H_2Ind]^-$ 657.6811 (657.6798), $[RuBr_4]^-$ 421.5753 (421.5736).

^{1}H NMR (500.10 MHz, DMSO-d_6): δ(cation) = 8.07 (s, 1H, H_c), 7.76 (d, $^3J_{H,H}$ = 8 Hz, 1H, H_d), 7.53 (d, $^3J_{H,H}$ = 8 Hz, 1H, H_g), 7.34 (dd, $^3J_{H,H}$ = 7 Hz, $^3J_{H,H}$ = 7 Hz, 1H, H_f), 7.10 (dd, $^3J_{H,H}$ = 7 Hz, $^3J_{H,H}$ = 7 Hz, 1H, H_e) ppm; δ(anion) = 3.30 (bs, 2H, H_5/H_6), 3.01 (bs, 2H, H_5/H_6), 2.30 (bs, 2H, H_4/H_7), 2.17 (bs, 2H, H_4/H_7), -8 (bs, 2H, H_1), -14.5 (bs, 2H, H_3) ppm.

Solubility: 0.39 mg/mL; 0.5 mM (in 1% DMSO)

Elemental analysis:

$C_{21}H_{19}Br_4N_6Ru \cdot 0.15\ H_2O\ 0.45\ HBr$	C [wt%]	H [wt%]	N [wt%]	O [wt%]
Calculated	30.94	2.44	10.31	0.29
Found	31.01	2.29	10.27	0.39
Δ	0.07	0.15	0.04	0.10

4.3.5 Synthesis of Caesium (*OC*-6-11)-tetrabromidobis(1*H*-indazole)ruthenate(III) (**2b**)

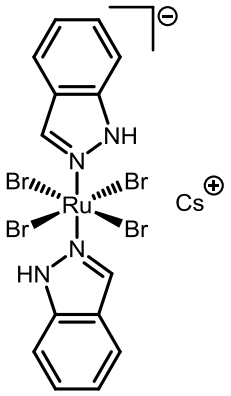

$C_{14}H_{12}Br_4CsN_4Ru$
M = 789.87 g/mol

Crude **2a** (1110 mg) was added to fine powdered CsBr (403 mg, 1.89 mmol, 3.3 eq.) and combined with a mixture of pure non-denatured ethanol (3 mL) and MEK (1 mL). The resulting suspension was stirred for 4 hours at room temperature, filtered and washed with ethanol (99%). Afterwards, the filtered material was suspended in a mixture of EtOH/H_2O (1.5 mL, 2:1, v/v), stirred for 15 minutes at room temperature, filtered, washed with ethanol and dried by suction. The obtained crude material contained residual indazolium.

The second step of the synthesis was performed according to the general procedure described in section 4.2.3, using the crude material previously obtained, CsBr (342 mg, 1.6 mmol, 2.8 eq.), a mixture of MEK (1 mL) and EtOH (0.9 mL) and a reaction time of 2 hours to form the solvate, a mixture of 1 mL EtOH with 0.5 mL H_2O and a reaction time of 15 minutes to form the hydrate. Upon mixing with aqueous ethanol, the purple material turned into a dark purple solid. The equivalents of CsBr and the yield are calculated based on employed $RuCl_3.xH_2O$ (150 mg, 0.57 mmol, 1.0 eq., calculated as $RuCl_3 \cdot 3H_2O$).

Yield: 281 mg (62 %), dark purple solid.

ESI-MS$^-$ *m/z* Found (Calculated): $[M–Cs]^-$ 657.6819 (657.6798), $[RuBr_4]^-$ 421.5745 (421.5736).

^{1}H NMR (500.10 MHz, DMSO-d_6): δ(anion) = 3.30 (bs, 2H, H_5/H_6), 3.01 (bs, 2H, H_5/H_6), 2.30 (bs, 2H, H_4/H_7), 2.16 (bs, 2H, H_4/H_7), -8 (bs, 2H, H_1), -14.5 (bs, 2H, H_3) ppm.

Elemental analysis:

$C_{14}H_{12}Br_4CsN_4Ru$	C [wt%]	H [wt%]	N [wt%]
Calculated	21.29	1.53	7.09
Found	21.04	1.53	6.78
Δ	0.25	0.00	0.31

4.3.6 Synthesis of Sodium (*OC*-6-11)-tetrabromidobis(1*H*-indazole)ruthenate(III) (**2c**)

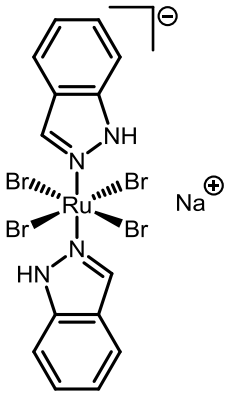

$C_{14}H_{12}Br_4N_4NaRu$
M = 679.95 g/mol

The synthesis was performed according to the general procedure described in section 4.2.4 with the exception that acetone was utilized for the extraction instead of acetonitrile. **2b** (281 mg, 0.36 mmol, 1.0 eq.), 2.8 mL 1.1 M $NaAl(SO_4)_2$, CsBr (8 mg, 0.04 mmol, 0.1 eq.) and a reaction time of 24 hours was employed. Afterwards, 6 mL sat. Na_2SO_4 were used for washing, 3 mL acetone for the extraction and 80 mL MTBE for the precipitation. Single crystals suitable for X-ray diffraction analysis were obtained from vapour diffusion of diethyl ether into a saturated ethyl acetate complex solution.

Yield: 84 mg (35%), brown-purple granular solid.

ESI-MS$^-$ *m/z* Found (Calculated): $[M–Na]^-$ 657.6812 (657.6798), $[RuBr_4]^-$ 421.5753 (421.5736).

^{1}H NMR (500.10 MHz, DMSO-d_6): δ(anion) = 3.30 (bs, 2H, H_5/H_6), 3.00 (bs, 2H, H_5/H_6), 2.30 (bs, 2H, H_4/H_7), 2.15 (bs, 2H, H_4/H_7), -8 (bs, 2H, H_1), -14.5 (bs, 2H, H_3) ppm.

Solubility: 1.41 mg/mL; 2.1 mM (in 1% DMSO)

4.3.7 Synthesis of Tetra(*n*-butyl)ammonium (*OC*-6-11)-tetrabromidobis(1*H*-indazole)ruthenate(III) (**2d**)

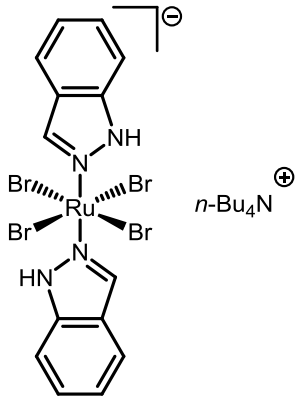

$C_{30}H_{48}Br_4N_5Ru$
M = 899.44 g/mol

2a (60 mg, 0.077 mmol 1.0 eq.) was dissolved in a mixture of acetone (5 mL) and H_2O (5 mL) by ultrasonic treatment and additional 40 mL H_2O were added. Afterwards, *n*-Bu_4NBr (100 mg, 0.31 mmol, 4.0 eq.) was added to the clear, stirred solution and immediate precipitation was observed. The mixture was stirred for 2 hours at room temperature and the solids were separated by filtration. The filtered material was thoroughly washed with water and dried *in vacuo*.

Yield: 61 mg (88%), dark pink solid.

ESI-MS$^-$ *m/z* Found (Calculated): $[M-n\text{-}Bu_4N]^-$ 657.69 (657.68), $[RuBr_4]^-$ 421.59 (421.57).

ESI-MS$^+$ *m/z* Found (Calculated): $[n\text{-}Bu_4N]^+$ 242.46 (242.47)

^{1}H NMR (500.10 MHz, MeOH-d_4): δ(cation) = 3.19–3.24 (m, 8H, N-CH_2), 1.62–1.75 (m, 8H, CH_2), 1.34–1.48 (m, 8H, CH_2), 1.02 (t, $^3J_{H,H}$ = 7 Hz, 12H, CH_3) ppm; δ(anion) = 3.78 (bs, 2H, H_5/H_6), 3.42 (bs, 2H, H_5/H_6), 3.17 (bs, 2H, H_4/H_7), 2.70 (bs, 2H, H_4/H_7), -12.8 (bs, 2H, H_3) ppm.

4.3.8 Synthesis of Tetraphenylphosphonium (*OC*-6-11)-tetrabromidobis(1*H*-indazole)ruthenate(III) (**2e**)

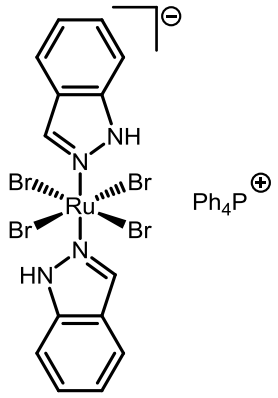

$C_{38}H_{32}Br_4N_4PRu$
M = 996.36 g/mol

2a (100 mg, 0.13 mmol 1 eq.) was dissolved in a mixture of methanol (15 mL) and H_2O (15 mL) by ultrasonicification and additional 150 mL H_2O were added. Afterwards, Ph_4PBr (216 mg, 0.52 mmol, 4.0 eq.) were added to the clear, stirred solution and immediate precipitation was observed. The mixture was stirred for 2 hours at room temperature and the solids were separated by filtration. The filtered material was thoroughly washed with water and dried *in vacuo*. Single crystals suitable for X-ray diffraction analysis were obtained from vapour diffusion of diethyl ether into a saturated dichloromethane complex solution.

Yield: 86 mg (67%), pink solid.

ESI-MS$^-$ *m/z* Found (Calculated): $[M - Ph_4P]^-$ 657.69 (657.68), $[RuBr_4]^-$ 421.58 (421.57).

ESI-MS$^+$ *m/z* Found (Calculated): $[Ph_4P]^+$ 339.14 (339.13)

^{1}H NMR (500.10 MHz, DMSO-d_6): δ(cation) = 7.14–7.21 (m, 8H, ArH_{ortho}), 6.92 (dd, $^3J_{H,H}$ = 7 Hz, $^3J_{H,H}$ = 7 Hz, 8H, ArH_{meta}), 6.78 (dd, $^3J_{H,H}$ = 7 Hz, $^3J_{H,H}$ = 7 Hz, 4H, ArH_{para}) ppm; δ(anion) = 3.30 (bs, 2H, H_5/H_6), 3.01 (bs, 2H, H_5/H_6), 2.30 (bs, 2H, H_4/H_7), 2.16 (bs, 2H, H_4/H_7), -8 (bs, 2H, H_1), -14.5 (bs, 2H, H_3) ppm.

4.3.9 Synthesis of Indazolium (*OC*-6-22)-tetrachloridobis(1*H*-indazole)rhodate(III) (*cis*-**4a**) and Indazolium (*OC*-6-11)-tetrachloridobis(1*H*-indazole)rhodate(III) (*trans*-**4a**)

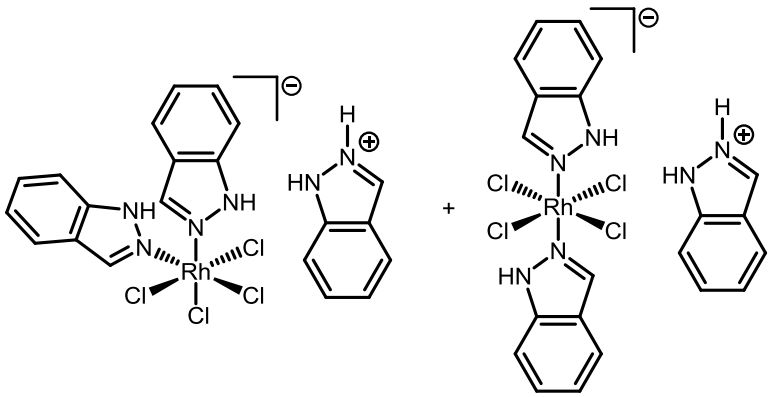

$C_{21}H_{19}Cl_4N_6Rh$
M = 600.13 g/mol

The synthesis was performed according to the general procedures described in sections 4.2.1 and 4.2.2, using $RhCl_3.xH_2O$ (100 mg, 0.38 mmol, 1.0 eq.) dissolved in 12 mL EtOH/HCl conc. and 1*H*-indazole (340 mg, 2.88 mmol, 7.6 eq.) dissolved in 5 mL concentrated HCl. After 16 hours of reaction time, the complex was stirred in 60 mL H_2O and isolated by filtration.

Yield: 175 mg (77%), pale yellow granular solid

ESI-MS$^-$ *m/z* Found (Calculated): $[M–H_2Ind]^-$ 480.87 (480.88), $[RhCl_4]^-$ 244.76 (244.71).

^{1}H NMR (500.10 MHz, DMSO-d_6): δ(cation) = 12.57 (s, 1H, H_a), 8.06 (s, 1H, H_c), 7.76 (d, $^3J_{H,H}$ = 8 Hz, 1H, H_d), 7.53 (d, $^3J_{H,H}$ = 8 Hz, 1H, H_g), 7.34 (dd, $^3J_{H,H}$ = 8 Hz, $^3J_{H,H}$ = 8 Hz, 1H, H_f), 7.10 (dd, $^3J_{H,H}$ = 8 Hz, $^3J_{H,H}$ = 8 Hz, 1H, H_e) ppm; δ(anion) = 12.79 and 12.78 (s, H_1), 8.77 and 8.41 (s, H_3), 7.89 and 7.84 (d, $^3J_{H,H}$ = 8 Hz, H_4), 7.77 and 7.74 (d, $^3J_{H,H}$ = 8 Hz, H_7), 7.42 and 7.37 (t, $^3J_{H,H}$ = 8 Hz, H_6), 7.20 and 7.13 (t, $^3J_{H,H}$ = 8 Hz, H_5) ppm. For the anion, the intensities are not available since the measured sample contained a mixture of products.

Elemental analysis:

$C_{21}H_{19}Cl_4N_6Rh \cdot 0.8$ HCl	C [wt%]	H [wt%]	N [wt%]
Calculated	40.08	3.17	13.35
Found	40.29	2.96	13.36
Δ	0.21	0.21	0.01

4.3.10 Synthesis of Caesium

(*OC*-6-22)-tetrachloridobis(1*H*-indazole)rhodate(III) (*cis*-**4b**) and

Caesium (*OC*-6-11)-tetrachloridobis(1*H*-indazole)rhodate(III) (*trans*-**4b**)

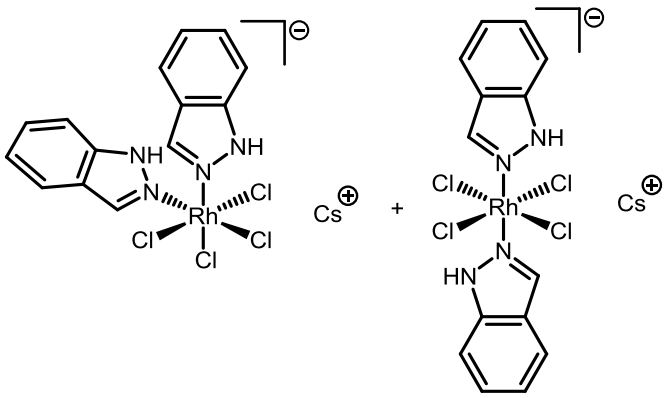

$C_{14}H_{12}Cl_4CsN_4Rh$
M = 613.89 g/mol

The synthesis was performed according to the general procedure described in section 4.2.3, using crude *cis/trans*-**4a** (293 mg), CsCl (361 mg, 2.14 mmol, 2.8 eq.), a mixture of MEK (1.6 mL) and EtOH (1.4 mL) and a reaction time of 16 hours to form the solvate, a mixture of 1 mL EtOH with 0.5 mL H_2O and a reaction time of 15 minutes to form the hydrate. The equivalents of CsCl and the yield are calculated from employed $RhCl_3.xH_2O$ (100 mg, 0.38 mmol, 1.0 eq., calculated as $RhCl_3 \cdot 3H_2O$).

Yield: 146 mg (63%), yellow-orange microcrystalline solid.

ESI-MS$^-$ *m/z* Found (Calculated): $[M-Cs]^-$ 480.87 (480.88), $[RhCl_4]^-$ 244.77 (244.71).

^{1}H NMR (500.10 MHz, DMSO-d_6): δ(anion) = 12.79 and 12.78 (s, H_1), 8.77 and 8.41 (s, H_3), 7.89 and 7.84 (d, $^3J_{H,H}$ = 8 Hz, H_4), 7.77 and 7.74 (d, $^3J_{H,H}$ = 8 Hz, H_7), 7.42 and 7.37 (dd, $^3J_{H,H}$ = 8 Hz, $^3J_{H,H}$ = 8 Hz, H_6), 7.20 and 7.13 (dd, $^3J_{H,H}$ = 8 Hz, $^3J_{H,H}$ = 8 Hz, H_5) ppm. For the anion, the intensities are not available since the measured sample contained a mixture of products.

Elemental analysis:

$C_{14}H_{12}Cl_4CsN_4Rh \cdot 1\ H_2O$	C [wt%]	H [wt%]	N [wt%]
Calculated	26.61	2.23	8.87
Found	26.48	2.12	8.60
Δ	0.13	0.11	0.27

4.3.11 Synthesis of Sodium (*OC*-6-22)-tetrachloridobis(1*H*-indazole)rhodate(III) (*cis*-**4c**) and Sodium (*OC*-6-11)-tetrachloridobis(1*H*-indazole)rhodate(III) (*trans*-**4c**)

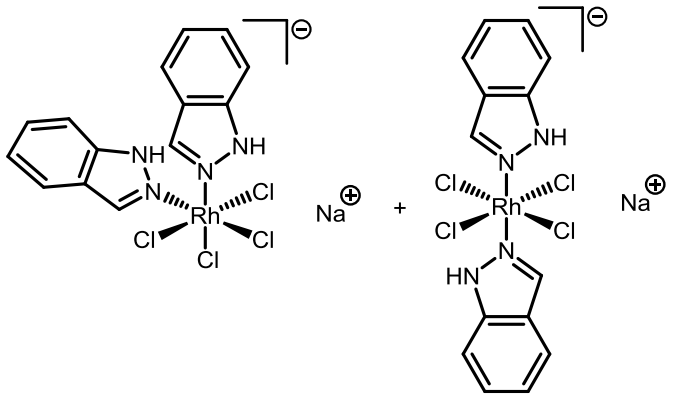

$C_{14}H_{12}Cl_4N_4NaRh$
M = 503.97 g/mol

The synthesis was performed according to the general procedure described in section 4.2.4, using *cis/trans*-**4b** (146 mg, 0.24 mmol, 1.0 eq.), 200 µL 1.1 M $NaAl(SO_4)_2$, CsCl (4 mg, 0.02 mmol, 0.1 eq.) and a reaction time of 48 hours. Afterwards, 6 mL sat. Na_2SO_4 were used for washing and 3 mL acetonitrile for the extraction.

For separation of the isomers, 2 mL MTBE were added to the acetonitrile complex solution and stored at 4 °C for 1 hour to complete precipitation of *trans*-**4c**. The isomer was isolated by filtration, thoroughly washed with MTBE and dried *in vacuo*. Afterwards, small portions of MTBE (1 mL) were added to the remaining acetonitrile solution and the respective precipitates analyzed *via* ^{1}H NMR. Pure fractions of *trans*-**4c** were isolated as described above. A small mixed fraction was discarded after addition of ~4 mL MTBE. The *cis* isomer was precipitated by the addition of further 12 mL MTBE and the mixture was stored at 4°C for 2 hours to complete the precipitation. To isolate *cis*-**4c**, the material was filtered, washed with MTBE and dried in vacuo. X-ray diffraction quality single crystals of *cis*-**4c** were selected directly from the precipitated solids after storage at 4 °C for 4 days.

Yield (*cis*-**4c**): 35 mg (29%), yellow microcrystalline solid.

Yield (*trans*-**4c**): 30 mg (25%), bright orange microcrystalline solid.

ESI-MS$^-$ (both isomers) *m/z* Found (Calculated): $[M-Na]^-$ 480.87 (480.88), $[RhCl_4]^-$ 244.74 (244.71).

^{1}H NMR *cis*-**4c** (700.40 MHz, DMSO-d_6): δ(anion) = 12.79 (s, 1H, H_1), 12.78 (s, 1H, H_1), 8.77 (s, 1H, H_3), 8.41 (s, 1H, H_3), 7.89 (d, $^3J_{H,H}$ = 8 Hz, 1H, H_4), 7.84 (d, $^3J_{H,H}$ = 8 Hz, 1H, H_7), 7.77 (d, $^3J_{H,H}$ = 8 Hz, 1H, H_4), 7.74 (d, $^3J_{H,H}$ = 8 Hz, 1H, H_7), 7.42 (dd, $^3J_{H,H}$ = 8 Hz, $^3J_{H,H}$ = 8 Hz, 1H, H_6), 7.37 (dd, $^3J_{H,H}$ = 8 Hz, $^3J_{H,H}$ = 8 Hz, 1H, H_6), 7.20 (dd, $^3J_{H,H}$ = 8 Hz, $^3J_{H,H}$ = 8 Hz, 1H, H_5), 7.13 (dd, $^3J_{H,H}$ = 8 Hz, 1H, H_5) ppm.

^{1}H NMR *trans*-**4c** (600.25 MHz, DMSO-d_6): δ(anion) = 12.78 (s, 2H, H_1), 8.41 (s, 2H, H_3),7.77 (d, $^3J_{H,H}$ = 8 Hz, 1H, H_4), 7.74 (d, $^3J_{H,H}$ = 8 Hz, 2H, H_7), 7.37 (dd, $^3J_{H,H}$ = 8 Hz, $^3J_{H,H}$ = 8 Hz, 2H, H_6), 7.14 (dd, $^3J_{H,H}$ = 8 Hz, $^3J_{H,H}$ = 8 Hz, 1H, H_5) ppm.

Elemental analysis (*trans*-**4c**):

$C_{14}H_{12}Cl_4CsN_4Rh \cdot 2\ H_2O$	C [wt%]	H [wt%]	N [wt%]
Calculated	31.14	2.99	10.38
Found	31.40	2.70	10.33
Δ	0.26	0.29	0.05

4.3.12 Synthesis of Sodium (*OC*-6-11)-tetrachloridobis(ethanedioato-κO^1,κO^2)ruthenate(III) (**5c**)

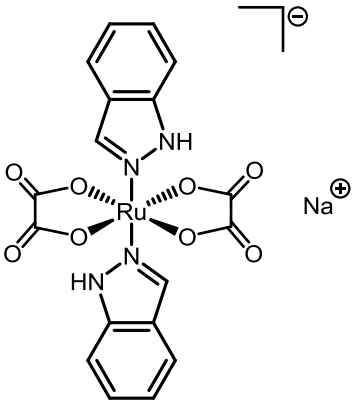

$C_{18}H_{12}N_4NaO_8Ru$
M = 536.37 g/mol

The following preparation was derived from a literature procedure.[106] Sodium oxalate (315 mg, 2.35 mmol, 1.0 eq.) was dissolved in 120 mL H_2O and silver nitrate (880 mg, 5.17 mmol, 2.2 eq.) was added to the stirred solution. After stirring for 1 hour under light protection, the formed silver oxalate was separated by filtration and washed thoroughly with H_2O and acetone (97% yield, 694 mg). The white solid was stored under light protection at room temperature.

1c (50 mg, 0.09 mmol, 1.0 eq.) was dissolved in acetonitrile (1 mL), precipitated with MTBE (9 mL), filtered and thoroughly washed with MTBE to remove excess H_2O and dried *in vacuo*. Silver oxalate (99 mg, 0.33 mmol, 3.5 equivalents) was suspended in dry methanol (10 mL), **1c** was added to the stirred mixture and the resulting suspension was stirred for 48 hours at room temperature under inert atmosphere and light protection. Afterwards, the suspension was filtered through Celite to remove the AgCl precipitate, and the Celite pad was washed with methanol (10 mL) in three portions. The filtrates were combined, and the solvent was removed under reduced pressure until ca. 4 mL solvent remained in the flask. Diethyl ether (4 mL) was added and the mixture stored at 4°C for 24 hours to complete precipitation. The solids were filtered and washed with diethyl ether.

Yield: 7 mg (14 %), bright red fine powdered solid.

ESI-MS$^-$ *m/z* Found (Calculated): $[M-Na]^-$ 513.9705 (513.9709), $[RhCl_4]^-$ 277.8632 (277.8637).

ESI-MS$^+$ *m/z* Found (Calculated): $[M+Na]^+$ 559.9492 (559.9494)

5 References

1. Cancer. https://www.who.int/westernpacific/health-topics/cancer.
2. *Jahrbuch der Gesundheitsstatistik 2017*. (Verlag Österreich GmbH, 2019).
3. Krebserkrankungen. http://www.statistik.at/web_de/statistiken/menschen_und_gesellschaft/gesundheit/krebserkrankungen/index.html.
4. STATcube - Tabellenansicht. https://statcube.at/statistik.at/ext/statcube/jsf/tableView/tableView.xhtml.
5. WORLD HEALTH ORGANIZATION: REGIONAL OFFICE FOR EUROPE. *WORLD CANCER REPORT: cancer research for cancer development.* (IARC, 2020).
6. Hahn, W. C. & Weinberg, R. A. Modelling the molecular circuitry of cancer. *Nat. Rev. Cancer* **2**, 331–341 (2002).
7. Anand, P. *et al.* Cancer is a Preventable Disease that Requires Major Lifestyle Changes. *Pharm. Res.* **25**, 2097–2116 (2008).
8. Lichtenstein, P. *et al.* Environmental and Heritable Factors in the Causation of Cancer — Analyses of Cohorts of Twins from Sweden, Denmark, and Finland. *N. Engl. J. Med.* **343**, 78–85 (2000).
9. Reitsma, M. B. *et al.* Smoking prevalence and attributable disease burden in 195 countries and territories, 1990–2015: a systematic analysis from the Global Burden of Disease Study 2015. *The Lancet* **389**, 1885–1906 (2017).
10. Hecht, S. S. & Szabo, E. Fifty Years of Tobacco Carcinogenesis Research: From Mechanisms to Early Detection and Prevention of Lung Cancer. *Cancer Prev. Res. (Phila. Pa.)* **7**, 1–8 (2014).
11. Weinberg, R. A. *The biology of cancer*. (Garland Science, Taylor & Francis Group, 2014).
12. Hanahan, D. & Weinberg, R. A. Hallmarks of Cancer: The Next Generation. *Cell* **144**, 646–674 (2011).
13. Fouad, Y. A. & Aanei, C. Revisiting the hallmarks of cancer. *Am. J. Cancer Res.* **7**, 1016–1036 (2017).
14. Ribatti, D. A revisited concept: Contact inhibition of growth. From cell biology to malignancy. *Exp. Cell Res.* **359**, 17–19 (2017).
15. Fernald, K. & Kurokawa, M. Evading apoptosis in cancer. *Trends Cell Biol.* **23**, 620–633 (2013).
16. von Morgen, P. & Maciejowski, J. The ins and outs of telomere crisis in cancer. *Genome Med.* **10**, 89 (2018).
17. Zuazo-Gaztelu, I. & Casanovas, O. Unraveling the Role of Angiogenesis in Cancer Ecosystems. *Front. Oncol.* **8**, 248 (2018).

18. Golombek, S. K. *et al.* Tumor targeting via EPR: Strategies to enhance patient responses. *Adv. Drug Deliv. Rev.* **130**, 17–38 (2018).

19. *Metastatic cancer: clinical and biological perspectives*. (Landes Bioscience, 2013).

20. Chabner, B. A. & Roberts, T. G. Chemotherapy and the war on cancer. *Nat. Rev. Cancer* **5**, 65–72 (2005).

21. Airley, R. *Cancer chemotherapy*. (Wiley-Blackwell, 2009).

22. *Pharmacology: principles and practice*. (Elsevier/Academic Press, 2009).

23. Schirrmacher, V. From chemotherapy to biological therapy: A review of novel concepts to reduce the side effects of systemic cancer treatment (Review). *Int. J. Oncol.* **54**, 407–419 (2019).

24. Baudino, T. Targeted Cancer Therapy: The Next Generation of Cancer Treatment. *Curr. Drug Discov. Technol.* **12**, 3–20 (2015).

25. Zoroddu, M. A. *et al.* The essential metals for humans: a brief overview. *J. Inorg. Biochem.* **195**, 120–129 (2019).

26. Dabrowiak, J. C. Metals in Medicine Special Issue. *Inorganica Chim. Acta* **393**, 1–2 (2012).

27. Alimoghaddam, K. A review of arsenic trioxide and acute promyelocytic leukemia. *Int. J. Hematol.-Oncol. Stem Cell Res.* **8**, 44–54 (2014).

28. Blodgett, R. C. & Pietrusko, R. G. Long-term efficacy and safety of auranofin: a review of clinical experience. *Scand. J. Rheumatol. Suppl.* **63**, 67–78 (1986).

29. for the International Group for Studies of Lithium (IGSLi) *et al.* Clinical use of lithium salts: guide for users and prescribers. *Int. J. Bipolar Disord.* **7**, 16 (2019).

30. Akbar, M. U., Ahmad, M. R., Shaheen, A. & Mushtaq, S. A review on evaluation of technetium-99m labeled radiopharmaceuticals. *J. Radioanal. Nucl. Chem.* **310**, 477–493 (2016).

31. Wahsner, J., Gale, E. M., Rodríguez-Rodríguez, A. & Caravan, P. Chemistry of MRI Contrast Agents: Current Challenges and New Frontiers. *Chem. Rev.* **119**, 957–1057 (2019).

32. Rosenberg, B., Van Camp, L. & Krigas, T. Inhibition of Cell Division in Escherichia coli by Electrolysis Products from a Platinum Electrode. *Nature* **205**, 698–699 (1965).

33. Rosenberg, B., Vancamp, L., Trosko, J. E. & Mansour, V. H. Platinum Compounds: a New Class of Potent Antitumour Agents. *Nature* **222**, 385–386 (1969).

34. Dasari, S. & Bernard Tchounwou, P. Cisplatin in cancer therapy: Molecular mechanisms of action. *Eur. J. Pharmacol.* **740**, 364–378 (2014).

35. Ho, G. Y., Woodward, N. & Coward, J. I. G. Cisplatin versus carboplatin: comparative review of therapeutic management in solid malignancies. *Crit. Rev. Oncol. Hematol.* **102**, 37–46 (2016).

36. Mehmood, R. K. Review of cisplatin and oxaliplatin in current immunogenic and monoclonal antibody treatments. *Oncol. Rev.* **8**, (2014).

37. Graham, J., Muhsin, M. & Kirkpatrick, P. Oxaliplatin. *Nat. Rev. Drug Discov.* **3**, 11–12 (2004).

38. Apps, M. G., Choi, E. H. Y. & Wheate, N. J. The state-of-play and future of platinum drugs. *Endocr. Relat. Cancer* **22**, R219–R233 (2015).

39. Dabrowiak, J. C. *Metals in Medicine*. (John Wiley & Sons, Ltd, 2009). doi:10.1002/9780470684986.

40. Makovec, T. Cisplatin and beyond: molecular mechanisms of action and drug resistance development in cancer chemotherapy. *Radiol. Oncol.* **53**, 148–158 (2019).

41. *Cancer chemotherapy and biotherapy: principles and practice*. (Wolters Kluwer Health/Lippincott Williams & Wilkins, 2011).

42. Miller, R. P., Tadagavadi, R. K., Ramesh, G. & Reeves, W. B. Mechanisms of Cisplatin Nephrotoxicity. *Toxins* **2**, 2490–2518 (2010).

43. Lokich, J. What Is the "Best" Platinum: Cisplatin, Carboplatin, or Oxaliplatin? *Cancer Invest.* **19**, 756–760 (2001).

44. Krauss, F. & Collier, W. A. Über die biologischen Wirkungen von anorganischen Stoffen: I. Mitteilung: Die Wirksamkeit verschiedener Schwermetallverbindungen auf Bakterien, Blutparasiten und den experimentellen Mäusekrebs. *Naunyn-Schmiedebergs Arch. Für Exp. Pathol. Pharmakol.* **162**, 452–462 (1931).

45. Lin, K., Zhao, Z.-Z., Bo, H.-B., Hao, X.-J. & Wang, J.-Q. Applications of Ruthenium Complex in Tumor Diagnosis and Therapy. *Front. Pharmacol.* **9**, 1323 (2018).

46. Antonarakis, E. S. & Emadi, A. Ruthenium-based chemotherapeutics: are they ready for prime time? *Cancer Chemother. Pharmacol.* **66**, 1–9 (2010).

47. Page, S. M., Boss, S. R. & Barker, P. D. Tuning heavy metal compounds for anti-tumor activity: is diversity the key to ruthenium's success? *Future Med. Chem.* **1**, 541–559 (2009).

48. Guo, W. *et al.* Transferrin Serves As a Mediator to Deliver Organometallic Ruthenium(II) Anticancer Complexes into Cells. *Inorg. Chem.* **52**, 5328–5338 (2013).

49. Timerbaev, A. R., Rudnev, A. V., Semenova, O., Hartinger, C. G. & Keppler, B. K. Comparative binding of antitumor indazolium [trans-tetrachlorobis(1H-indazole)ruthenate(III)] to serum transport proteins assayed by capillary zone electrophoresis. *Anal. Biochem.* **341**, 326–333 (2005).

50. Lentz, F. *et al.* Pharmacokinetics of a novel anticancer ruthenium complex (KP1019, FFC14A) in a phase I dose-escalation study: *Anticancer. Drugs* **20**, 97–103 (2009).

51. Durig, J. R., Danneman, J., Behnke, W. D. & Mercer, E. E. The induction of filamentous growth in Escherichia coli by ruthenium and palladium complexes. *Chem. Biol. Interact.* **13**, 287–294 (1976).

52. Meier-Menches, S. M., Gerner, C., Berger, W., Hartinger, C. G. & Keppler, B. K. Structure–activity relationships for ruthenium and osmium anticancer agents – towards clinical development. *Chem. Soc. Rev.* **47**, 909–928 (2018).

53. Pötsch, I., Baier, D., Keppler, B. K. & Berger, W. CHAPTER 12. Challenges and Chances in the Preclinical to Clinical Translation of Anticancer Metallodrugs. in *Metallobiology* (eds. Casini, A., Vessières, A. & Meier-Menches, S. M.) 308–347 (Royal Society of Chemistry, 2019). doi:10.1039/9781788016452-00308.

54. Aird, R. E. *et al.* In vitro and in vivo activity and cross resistance profiles of novel ruthenium (II) organometallic arene complexes in human ovarian cancer. *Br. J. Cancer* **86**, 1652–1657 (2002).

55. Scolaro, C. *et al.* In Vitro and in Vivo Evaluation of Ruthenium(II)–Arene PTA Complexes. *J. Med. Chem.* **48**, 4161–4171 (2005).

56. Wang, F. *et al.* Controlling ligand substitution reactions of organometallic complexes: Tuning cancer cell cytotoxicity. *Proc. Natl. Acad. Sci.* **102**, 18269–18274 (2005).

57. Wu, B., Dröge, P. & Davey, C. A. Site selectivity of platinum anticancer therapeutics. *Nat. Chem. Biol.* **4**, 110–112 (2008).

58. Boros, E., Dyson, P. J. & Gasser, G. Classification of Metal-Based Drugs according to Their Mechanisms of Action. *Chem* **6**, 41–60 (2020).

59. Monro, S. *et al.* Transition Metal Complexes and Photodynamic Therapy from a Tumor-Centered Approach: Challenges, Opportunities, and Highlights from the Development of TLD1433. *Chem. Rev.* **119**, 797–828 (2019).

60. Keppler, B. K. *et al.* Synthesis, molecular structure, and tumor-inhibiting properties of imidazolium trans-bis(imidazole)tetrachlororuthenate(III) and its methyl-substituted derivatives. *Inorg. Chem.* **26**, 4366–4370 (1987).

61. Keppler, B. K. & Rupp, W. Antitumor activity of imidazolium-bisimidazole-tetrachlororuthenate (III): A representative of a new class of inorganic antitumor agents. *J. Cancer Res. Clin. Oncol.* **111**, 166–168 (1986).

62. Berger, M. R., Garzon, F. T., Keppler, B. K. & Schmähl, D. Efficacy of new ruthenium complexes against chemically induced autochthonous colorectal carcinoma in rats. *Anticancer Res.* **9**, 761–765 (1989).

63. Keppler, B. K. *et al.* New Ruthenium Complexes for the Treatment of Cancer. in *Ruthenium and Other Non-Platinum Metal Complexes in Cancer Chemotherapy* (eds. Baulieu, E. et al.) vol. 10 41–69 (Springer Berlin Heidelberg, 1989).

64. Hartinger, C. G. *et al.* From bench to bedside – preclinical and early clinical development of the anticancer agent indazolium trans-[tetrachlorobis(1H-indazole)ruthenate(III)] (KP1019 or FFC14A). *J. Inorg. Biochem.* **100**, 891–904 (2006).

65. Peti, W., Pieper, T., Sommer, M., Keppler, B. K. & Giester, G. Synthesis of tumor-inhibiting complex salts containing the anion trans-

tetrachlorobis(indazole)ruthenate(III) and crystal structure of the tetraphenylphosphonium salt. *Eur. J. Inorg. Chem.* 1551–1555 (1999).

66. Burris, H. A. *et al.* Safety and activity of IT-139, a ruthenium-based compound, in patients with advanced solid tumours: a first-in-human, open-label, dose-escalation phase I study with expansion cohort. *ESMO Open* **1**, e000154 (2017).
67. FDA grants orphan drug designation to IT-139 for pancreatic cancer. https://www.healio.com/news/hematology-oncology/20170620/fda-grants-orphan-drug-designation-to-it139-for-pancreatic-cancer.
68. Zhang, Y., Sun, T. & Jiang, C. Biomacromolecules as carriers in drug delivery and tissue engineering. *Acta Pharm. Sin. B* **8**, 34–50 (2018).
69. Trondl, R. *et al.* NKP-1339, the first ruthenium-based anticancer drug on the edge to clinical application. *Chem Sci* **5**, 2925–2932 (2014).
70. Kratz, F. Albumin as a drug carrier: Design of prodrugs, drug conjugates and nanoparticles. *J. Controlled Release* **132**, 171–183 (2008).
71. Sulyok, M. *et al.* Two dimensional separation schemes for investigation of the interaction of an anticancer ruthenium(iii) compound with plasma proteins. *J. Anal. At. Spectrom.* **20**, 856 (2005).
72. Bijelic, A., Theiner, S., Keppler, B. K. & Rompel, A. X-ray Structure Analysis of Indazolium *trans*- [Tetrachlorobis(1 *H* -indazole)ruthenate(III)] (KP1019) Bound to Human Serum Albumin Reveals Two Ruthenium Binding Sites and Provides Insights into the Drug Binding Mechanism. *J. Med. Chem.* **59**, 5894–5903 (2016).
73. Bernhard K. Keppler *et al.* Binding of ruthenium(III) anti-tumor drugs to human lactoferrin probed by high resolution X-ray crystallographic structure analyses. *JBIC J. Biol. Inorg. Chem.* **1**, 424–431 (1996).
74. Cetinbas, N., Webb, M. I., Dubland, J. A. & Walsby, C. J. Serum-protein interactions with anticancer Ru(III) complexes KP1019 and KP418 characterized by EPR. *JBIC J. Biol. Inorg. Chem.* **15**, 131–145 (2010).
75. Clarke, M. J. *et al.* Chemical Considerations in the Design of Ruthenium Anticancer Agents. in *Platinum and Other Metal Coordination Compounds in Cancer Chemotherapy* (ed. Nicolini, M.) 582–600 (Springer US, 1988). doi:10.1007/978-1-4613-1717-3_65.
76. Cebrián-Losantos, B. *et al.* Synthesis and Reactivity of the Aquation Product of the Antitumor Complex *trans* -[Ru ^{III} Cl $_4$ (indazole) $_2$] $^-$. *Inorg. Chem.* **47**, 6513–6523 (2008).
77. Clarke, M. J. Ruthenium metallopharmaceuticals. *Coord. Chem. Rev.* **232**, 69–93 (2002).
78. Groessl, M. *et al.* Structure–Activity Relationships for NAMI-A-type Complexes (HL)[*trans* -RuCl $_4$ L(*S* -dmso)ruthenate(III)] (L = Imidazole, Indazole, 1,2,4-Triazole, 4-Amino-1,2,4-triazole, and 1-Methyl-1,2,4-triazole): Aquation, Redox Properties, Protein Binding, and Antiproliferative Activity. *J. Med. Chem.* **50**, 2185–2193 (2007).

79. Groessl, M., Hartinger, C. G., Dyson, P. J. & Keppler, B. K. CZE–ICP-MS as a tool for studying the hydrolysis of ruthenium anticancer drug candidates and their reactivity towards the DNA model compound dGMP. *J. Inorg. Biochem.* **102**, 1060–1065 (2008).

80. Blazevic, A. *et al.* Electronic State of Sodium trans-[Tetrachloridobis(1H-indazole)ruthenate(III)] (NKP-1339) in Tumor, Liver and Kidney Tissue of a SW480-bearing Mouse. *Sci. Rep.* **7**, 40966 (2017).

81. Hummer, A. A. *et al.* X-ray Absorption Near Edge Structure Spectroscopy to Resolve the in Vivo Chemistry of the Redox-Active Indazolium *trans* -[Tetrachlorobis(1 *H* -indazole)ruthenate(III)] (KP1019). *J. Med. Chem.* **56**, 1182–1196 (2013).

82. Schoenhacker-Alte, B. *et al.* Sensitivity towards the GRP78 inhibitor KP1339/IT-139 is characterized by apoptosis induction via caspase 8 upon disruption of ER homeostasis. *Cancer Lett.* **404**, 79–88 (2017).

83. Bakewell, S. J. *et al.* Suppression of stress induction of the 78-kilodalton glucose regulated protein (GRP78) in cancer by IT-139, an anti-tumor ruthenium small molecule inhibitor. *Oncotarget* **9**, 29698–29714 (2018).

84. Webb, M. I. *et al.* Increasing the Bioavailability of Ru ^{III} Anticancer Complexes through Hydrophobic Albumin Interactions. *Chem. - Eur. J.* **19**, 17031–17042 (2013).

85. Chang, Stephanie. W. *et al.* CF_3 Derivatives of the Anticancer Ru(III) Complexes KP1019, NKP-1339, and Their Imidazole and Pyridine Analogues Show Enhanced Lipophilicity, Albumin Interactions, and Cytotoxicity. *Inorg. Chem.* **55**, 4850–4863 (2016).

86. Reisner, E. *et al.* Tuning of Redox Potentials for the Design of Ruthenium Anticancer Drugs – an Electrochemical Study of [*trans* -$RuCl_4$L(DM *S* O)] $^-$ and [*trans* -$RuCl_4L_2$] $^-$ Complexes, where L = Imidazole, 1,2,4-Triazole, Indazole. *Inorg. Chem.* **43**, 7083–7093 (2004).

87. Kuhn, P.-S. *et al.* Improved reaction conditions for the synthesis of new NKP-1339 derivatives and preliminary investigations on their anticancer potential. *Dalton Trans.* **44**, 659–668 (2015).

88. Reedijk, J. Fast and slow versus strong and weak metal–DNA binding: consequences for anti-cancer activity. *Metallomics* **4**, 628 (2012).

89. Vojkovsky, T., Sill, K. & Carie, A. Manufacture of trans-[tetrachlorobis(1h-indazole)ruthenate (iii)] and compositions thereof. (2018).

90. Lipponer, K.-G., Vogel, E. & Keppler, B. K. Synthesis, Characterization and Solution Chemistry of trans-Indazoliumtetrachlorobis(Indazole)Ruthenate(III), a New Anticancer Ruthenium Complex. IR, UV, NMR, HPLC Investigations and Antitumor Activity. Crystal Structures of trans-1-Methyl-Indazoliumtetrachlorobis-(1-Methylindazole)Ruthenate(III) and its Hydrolysis Product trans-Monoaquatrichlorobis-(1-Methylindazole)-Ruthenate(III). *Met.-Based Drugs* **3**, 243–260 (1996).

91. Crutchley, R. J., Lever, A. B. P. & Poggi, A. Bis(bipyrazine)ruthenium(II) complexes: characterization, spectroscopy, and electrochemistry. *Inorg. Chem.* **22**, 2647–2650 (1983).

92. *Synthetic coordination chemistry: principles and practice*. (World Scientific, 1996).

93. Galanski, M., Arion, V., Jakupec, M. & Keppler, B. Recent Developments in the Field of Tumor-Inhibiting Metal Complexes. *Curr. Pharm. Des.* **9**, 2078–2089 (2003).

94. Sarma, U. C. & Poddar, R. K. Complexes of ruthenium(II) and -(III) with dimethylsulphoxide—III. Bis-iodo-tetrakis- dimethylsulphoxide ruthenium(II) and some other iodo complexes of ruthenium(II). *Polyhedron* **7**, 2627–2633 (1988).

95. Vock, C. A., Renfrew, A. K., Scopelliti, R., Juillerat-Jeanneret, L. & Dyson, P. J. Influence of the Diketonato Ligand on the Cytotoxicities of [Ru(η6-p-cymene)(R2acac)(PTA)]+ Complexes (PTA = 1,3,5-triaza-7-phosphaadamantane). *Eur. J. Inorg. Chem.* **2008**, 1661–1671 (2008).

96. Fernández, R., Melchart, M., Habtemariam, A., Parsons, S. & Sadler, P. J. Use of Chelating Ligands to Tune the Reactive Site of Half-Sandwich Ruthenium(II)–Arene Anticancer Complexes. *Chem. - Eur. J.* **10**, 5173–5179 (2004).

97. Groessl, M., Hartinger, C. G., Dyson, P. J. & Keppler, B. K. CZE–ICP-MS as a tool for studying the hydrolysis of ruthenium anticancer drug candidates and their reactivity towards the DNA model compound dGMP. *J. Inorg. Biochem.* **102**, 1060–1065 (2008).

98. Pieper, T., Peti, W. & Keppler, B. K. Solvolysis of the Tumor-Inhibiting Ru(III)-Complex trans-Tetrachlorobis(Indazole)Ruthenate(III). *Met.-Based Drugs* **7**, 225–232 (2000).

99. Gerweck, L. E. Tumor pH: Implications for treatment and novel drug design. *Semin. Radiat. Oncol.* **8**, 176–182 (1998).

100. Cebrián-Losantos, B. *et al.* Synthesis and Reactivity of the Aquation Product of the Antitumor Complex *trans*-[$Ru^{III}Cl_4(indazole)_2]^-$. *Inorg. Chem.* **47**, 6513–6523 (2008).

101. Rousseau, V. & Lindwall, H. G. Structure and Ultraviolet Absorption Spectra of Indazole, 3-Substituted Indazole and Some of Their Derivatives [1]. *J. Am. Chem. Soc.* **72**, 3047–3051 (1950).

102. Küng, A., Pieper, T., Wissiack, R., Rosenberg, E. & Keppler, B. K. Hydrolysis of the tumor-inhibiting ruthenium(III) complexes HIm trans-[RuCl4(im)2] and HInd trans-[RuCl4(ind)2] investigated by means of HPCE and HPLC-MS. *JBIC J. Biol. Inorg. Chem.* **6**, 292–299 (2001).

103. Fulmer, G. R. *et al.* NMR Chemical Shifts of Trace Impurities: Common Laboratory Solvents, Organics, and Gases in Deuterated Solvents Relevant to the Organometallic Chemist. *Organometallics* **29**, 2176–2179 (2010).

104. Stoll, V. S. & Blanchard, J. S. Chapter 6 Buffers. in *Methods in Enzymology* vol. 463 43–56 (Elsevier, 2009).

105. *Handbook of electrochemistry*. (Elsevier, 2007).

106. Ang, W. H. *et al.* Development of Organometallic Ruthenium–Arene Anticancer Drugs That Resist Hydrolysis. *Inorg. Chem.* **45**, 9006–9013 (2006).

6 Appendix

6.1 List of Abbreviations

°	degree
°C	degree centigrade
$^1O_2$	singlet oxygen
Å	Ångström, 10^{-10} m
δ	chemical shift (NMR)
CV	cyclic voltammetry
d	doublet (NMR)
dd	doublet of doublets (NMR)
D_2O	deuterated oxide
DMSO	dimethyl sulfoxide
DMSO-d_6	deuterated dimethyl sulfoxide
DNA	desoxyribonucleic acid
e.g.	*exempli gratia* (for example)
GRP 78	78 kDa glucose regulated protein
eq	equivalents
EtOAc	ethyl acetate
ESI	electrospray ionization
E. coli.	*Escherichia coli*
et al.	*et alii* (and others)
EtOH	ethanol
FDA	US Food and Drug administration agency
g	gram
h	hour
Hz	hertz (s^{-1})
HIm	1*H*-imidazole
HInd	1*H*-indazole
HSA	human serum albumin
i.e.	*id est* (that is to say)
J	Coupling constant (NMR)
K	Kelvin

k_{H2O}	reaction rate constant of hydrolysis
M	molar (mol/L)
M	molecular ion (mass spectrometry)
M^{III}	trivalent metal
MEK	methyl ethyl ketone
MeOH	methanol
MEOH-d_4	deuterated methanol
min	minute
MRI	magnetic resonance imaging
MS	mass spectrometry
MTBE	methyl *tert*-butyl ether
MTD	maximum tolerated dose
m/z	mass to charge ratio
nm	nanometer
NMR	nuclear magnetic resonance
PBS	phosphate-buffered saline
PTD	photodynamic therapy
pH	*pondus hydrogenii*
ppm	parts per million
RAPTA	ruthenium(II) arene PTA
s	singlet (NMR)
t	triplet (NMR)
Tf	transferrin
THF	tetrahydrofuran
UV-vis	ultraviolet-visible light
XANES	X-ray absorption near edge structure spectroscopy
X-ray	X-radiation

6.2 List of Figures